prolyl-hydroxylated protein, prolyl-hydroxylase genes were simultaneously introduced to the silkworms along with the recombinant protein gene. The resulting silkworms produced a protein containing a prolyl-hydroxylated collagen sequence in their cocoons (Adachi et al., 2006). While these studies demonstrated the possibility of mass production of recombinant collagens in transgenic silkworms, we recognized an important issue that needed to be addressed: given that the recombinant protein was incorporated into insoluble silk fibers, the protein could not be extracted without using strong chaotropic reagents.

Silk fibers are composed mainly of two types of protein: fibroin and sericin. The former comprises 70–80% of all silk proteins, constitutes the core of insoluble silk fibers, and is synthesized in the posterior silk glands (PSGs). Sericin, which accounts for 20–30% of silk proteins, refers to a group of hydrophilic glue proteins that surround the fibroin core and are synthesized in the middle silk glands (MSGs; Garel et al., 1997; Grzelak, 1995). The above-described recombinant fusion protein containing the collagen sequence was expressed in the PSGs, resulting in production of the recombinant protein into the insoluble fibroin core (Tomita et al., 2005). Recently, we also developed a sericin promoter-driven recombinant protein expression system, in which recombinant proteins are expressed in the MSGs and secreted into hydrophilic sericin layers of silk fibers. Green fluorescent protein (Tomita et al., 2007), human serum albumin (Ogawa et al., 2007), and mouse IgG (Iizuka et al., 2009) were successfully produced in cocoons. These proteins were extractable from cocoons by soaking them in mild neutral aqueous solutions such as phosphate-buffered saline (PBS) or Tris-buffered saline.

In this study, we generated transgenic silkworms that expressed the full-length triple helical region of the human type I collagen α1 chain [α1(I) chain] in the MSGs. Type I collagen is the most abundant fibril-forming collagen in the human body. A common form of type I collagen is a heterotrimer composed of two α1(I) chains and one α2(I) chain. It is also known that α1(I) chains are able to form a homotrimer in the absence of α2(I) chain (Nicholls et al., 1979). The recombinant α1(I) chain expressed in the MSGs was efficiently secreted into cocoons and was easily recoverable. Given that the silk glands had no prolyl-hydroxylase activity, the chains contained no hydroxyproline residues. In addition, the recombinant α1(I) chain expressed in this study lacks the telopeptide and propeptide promoting triple helix formation (Doege and Fessler, 1986; Olsen et al., 2001; Rosenbloom et al., 1976). Therefore, the α1(I) chains did not form the homotrimer with the triple helical structure, and their physio-chemical properties were similar to those of gelatin rather than collagen. We tested the possibility of using the recombinant α1(I) chain as a cell culture scaffold, and found that cells could be cultured on the chain as on marketed gelatin. As the recombinant α1(I) chain has uniform molecular weight and no risks of animal-derived pathogen contamination, the recombinant chain may be useful as a high-quality and safe substitute for marketed gelatin.

Materials and Methods

Experimental Animals

A strain of silkworm, pnd-w1, was obtained from the National Institute of Agrobiological Science (Tsukuba, Japan). Larvae were reared at 25°C on an artificial diet (Nosan Corporation, Yokohama, Japan).

Vector Construction for Transgenic Silkworms

The vector COL1A1/pMSG for transgenic silkworms was constructed using a full-length cDNA coding for the pro α1 chain of human type I procollagen (GenBank Accession No. Z74615) obtained by RT-PCR from human placenta total RNA (Clontech, Palo Alto, CA). The PCR-amplified product was cloned into the pCR4-TOPO vector (Invitrogen, Carlsbad, CA) using a TOPO cloning system (Invitrogen), which yielded pCR4COL1A1. To obtain the DNA fragment containing the baculovirus polyhedrin 5′-untranslated region (UTR; nt 140–189; GenBank Accession No. M30925; Iizuka et al., 2008), the signal sequence of human calreticulin (nt 109–159; GenBank Accession No. M84739), and the cDNA for the triple helical region of the α1(I) chain (nt 654–3695; Fig. 1A), PCR was performed using pCR4COL1A1 as a template. A set of primers, calSP/COL1A1-F (5′-ATGCTGCTATCCGTGCCGTTGCTGCTC-GGCCTCCTCGGCCTGGCCGTCGCCGGCCCCATGGGT-CCCTCT-3′) and *Nru*I/STP/COL1A1-R (5′-TCGCGATT-AGGGAGGACCAGGG-GGACC-3′), was used for the first PCR. A second PCR was performed using the product of the first PCR as a template and *Nru*I/Bm5UTR/calSP-F (5′-TCGCGAAAGTATTTTACTGTTTTCGTAACAGTTTT-GTAATAAAAAAACCTATAAATATGCTGCTATCCGTG-CCG-3′) and *Nru*I/STP/COL1A1-R as a primer set. The amplified product was cloned into the pCR4-TOPO vector to generate pCR4BmUTRcalSPCOL1A1. The DNA fragment was re-excised from pCR4BmUTRcalSPCOL1A1 by digestion with *Nru*I, and inserted between the *Bombyx mori* sericin 1 promoter and the fibroin light chain 3′-flanking sequence of pMSG1.1MG (Iizuka et al., 2009), giving rise to COL1A1/pMSG (Fig. 1B).

A vector carrying the gene of baculovirus trans-activator IE1 (Tomita et al., 2007) was prepared as follows. To obtain the DNA fragment consisting of the polyhedrin 5′-UTR and the IE1 gene, PCR was performed using pIE1 (Tomita et al., 2007) as a template. A set of primers, *Eco*RV/Bm5UTR/IE1-F (5′-GATATCAAGTATTTTACTGTTTTC-GTAACAGTTTTGTAATAAAAAAACCTATAAATATGA-CGCAAATTAATTTTAACGCGTCG-3′) and *Bgl*/IE1-R (5′-AGATCTTTAATTAAATTCAAATTTTTTATATTTACAA-TTTAG-3′), was used for the PCR. The amplified product

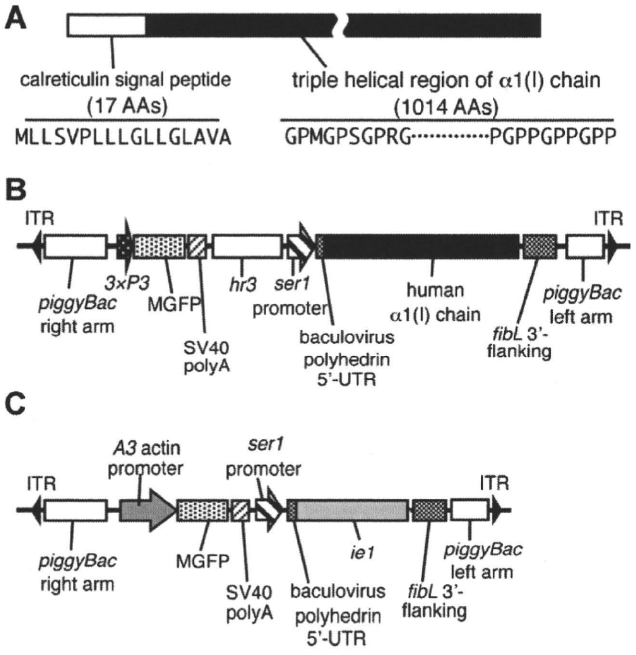

Figure 1. The structure of the transformation vector. **A**: The structure of the amino acid sequence of the α1(I) chain. The sequence of the α1(I) chain consists of a 17 amino acid (AA)-long calreticulin signal peptide (open box) and a 1,014 AA-long triple helical region of the α1(I) chain (filled box). **B**: The structure of the transformation vector COL1A1/pMSG. COL1A1/pMSG contained two expression units between the right and left arms of *piggyBac* as follows: *3xP3* promoter-driven MGFP cDNA with the SV40 polyA signal sequence (SV40 polyA) and the baculovirus-derived enhancer *hr3*-linked sericin 1 (*ser1*) promoter-driven α1(I) chain cDNA with the fibroin light chain gene polyA signal sequence (*fibL* 3′-flanking). ITR, inverted terminal repeat. **C**: Transformation vector pIM1. pIM1 contained two expression units between the right and left arms of *piggyBac* as follows: *Bombyx mori A3* actin promoter-driven MGFP cDNA with the SV40 polyA and *ser1* promoter-driven *ie1* gene with the *fibL* 3′-flanking.

was cloned into pCRII-TOPO vector (Invitrogen) to generate pCRBmUTRie1. The DNA fragment was released from pCRBmUTRie1 by digestion with *Eco*RV, and inserted between the *B. mori* sericin1 promoter and the fibroin light chain 3′-flanking sequence of pMSG1.1A3-MG, which had been created by replacing the *3xP3* promoter with the *B. mori A3* actin promoter (nt 1757–2595, GenBank Accession No. U49854) in pMSG1.1MG. The resulting vector was termed pIM1 (Fig. 1C).

Generation of Transgenic Silkworms

COL1A1/pMSG was injected with the helper vector pHA3PIG (Tamura et al., 2000) into pre-blastoderm embryos as described previously (Tomita et al., 2003). Hatched G_0 larvae were reared at 25°C to the moth stage. G_1 embryos obtained by sibling mating were screened for the expression of Monster Green Fluorescent Protein (MGFP; Promega, San Luis Obispo, CA) in the eyes and nervous tissues to obtain transgenic silkworms.

pIM1 was injected into eggs, and transgenic silkworms were created as described above, except that screening was performed by observing MGFP fluorescence in the larval body. The resulting transgenic silkworm (IM1) was crossed with silkworms carrying the α1(I) chain to obtain silkworms hemizygous for both the IE1 and the α1(I) chain genes.

To generate silkworms homozygous for the IE1 and the α1(I) chain genes, the above hemizygous silkworms were crossed with one another. From the next generations, homozygous silkworms for both genes were screened by genomic PCR using DNA extracted from blood cells as a template. Primers used in this PCR were designed from the genomic sequences flanking the transgene insertions, which were determined with an APA Transgene Locator Kit (BIO S&T Inc., Montreal, QC, Canada) according to the manufacturer's instructions.

SDS–PAGE and Western Blotting

Proteins in the sericin layer of silk fibers were extracted by incubating cocoons at 80°C for 5 min in a buffer consisting of 8 M urea, 2% 2-mercaptoethanol, and 50 mM Tris–HCl, pH 8.0. After centrifugation at 23,500*g* for 5 min, the obtained supernatant was electrophoresed on 0.1% SDS/5–20% polyacrylamide gradient gels (Atto, Tokyo, Japan) in running buffer (0.1% SDS, 12.5 mM Tris, and 125 mM glycine). The gels were stained with CBB-R250, and densitometric analyses were performed using the image-processing program, ImageJ (http://rsb.info.nih.gov/ij/). For Western blotting, the proteins on the gels were transferred onto PVDF membranes (Immobilon-P; Millipore, Billerica, MA), reacted with antihuman/bovine type I collagen antibodies (LB-1190; Cosmo Bio, Tokyo, Japan) and then with horseradish peroxidase (HRP)-linked anti-(rabbit IgG) antibodies (Cell Signaling Technology, Danvers, MA). The antigen–antibody complexes were visualized using the ECL Western Blotting Detection System (GE Healthcare, Little Chalfont, Buckinghamshire, UK).

Purification of the Recombinant α1(I) Chain From Transgenic Silkworm Cocoons

Cocoons were crushed into powder using a mill, suspended in a solution of 8 M urea and 0.5 M CH_3COOH, pH 2.0, at a concentration of 10 mg powdered cocoons/mL, and incubated at 4°C for 2 days with stirring. The resulting solution was filtered through filter paper and 70-μm nylon mesh. The solution was concentrated approximately threefold with an ultrafiltration membrane (Millipore) and urea was removed from the solution by adding 0.5 M CH_3COOH, pH 2.0, and subsequent ultrafiltration. NaCl was then added to the solution at a concentration of 0.5 M, and precipitated sericin was removed by centrifugation. Next, the recombinant α1(I) chain in the solution was collected by the addition of 3.5 M NaCl. The precipitate was

solubilized in 0.5 M CH_3COOH and subjected to dialysis against water.

N-Terminal Sequencing and Measurement of Amino Acid Composition

The N-terminal sequences of the purified α1(I) chain were determined with a G1000A protein sequencer (Hewlet Packard, Palo Alto, CA) using the standard protocol of Edman degradation. For the degradation reaction, 36 pmol of the chain were loaded onto the sequencer and the reaction was carried out for five cycles.

The purified α1(I) chain was hydrolyzed in 6 N HCl for 22 h at 110°C under vacuum, and analyzed for amino acid composition using a Hitachi 835 amino acid analyzer (Hitachi, Tokyo, Japan).

Determination of Melting and Gelation Points

The purified α1(I) chain was dissolved in distilled water at a concentration of 50 mg/mL, and the solution was subjected to determination of gelation and melting points as follows. The α1(I) chain solution was gradually cooled from 35 to −5°C at a rate of 1°C/min with a thermal cycler (Atto). The gelation point was determined by reading the temperature of the sample when its fluidity disappeared. For the analysis of the melting point, the α1(j) chain solution was incubated in icy water for 30 min to create a gel. The α1(I) chain gel was gradually heated from 0 to 40°C at a rate of 1°C/min with the thermal cycler. The melting point was determined by reading the temperature of the sample when the bubble at the bottom of the tube reached the surface of the sample solution.

Measurement of Circular Dichroism (CD) Spectra

CD spectra were recorded for the recombinant α1(I) chain using a spectropolarimeter J-820 (Jasco, Tokyo, Japan). The purified α1(I) chain was dissolved in 50 mM CH_3COOH at a concentration of 100 μg/mL for measurement in far ultraviolet (190–240 nm) regions, and the solution was placed in a cuvette with 2-mm pass length. The temperature was kept at 4°C during the procedures. Measurements were performed three times and the averaged values were plotted. Thermal transition curves were recorded by measuring molar ellipticity at 224 nm between 5 and 60°C at a rate of 30°C/h. The denaturing temperature was calculated with J-820 software (Jasco).

Endotoxin Test

An endotoxin level of the recombinant α1(I) chain was quantified using the limulus amebocyte lysate (LAL) as per the manufacturer's instructions (Endospecy ES-50M and Toxicolor DIA-MP; Seikagaku Biobusiness, Tokyo, Japan). Briefly, 50 μL standards or samples diluted with endotoxin-free water were mixed with LAL and incubated at 37°C for 30 min. After the substrate solution was added, the absorbance at 545 nm was measured. A standard curve was constructed by using the standards in the range of 0.02–0.1 EU/mL, and the concentration of endotoxin in each sample was determined by plotting the absorbance to the standard curve.

Quantifying the Spread of Human Dermal Skin Fibroblasts

The cell adhesivity to the recombinant α1(I) chain was analyzed by a quantitative cell-spreading assay using human dermal skin fibroblasts (HSFs; Kurabo, Osaka, Japan) as described previously (Yamada and Kennedy, 1984). In brief, a 96-well tissue culture plate (Becton Dickinson Labware, Franklin Lakes, NJ) was incubated with the recombinant α1(I) chain at various concentrations (0.31, 0.62, 1.25, 2.5, and 5.0 μg/mL) at 37°C for 1 h, treated with heat-denatured 0.5% bovine serum albumin to block the direct interaction between cells and the plate surface, and extensively washed with PBS. HSFs were seeded on the wells at a density of 1×10^4 cells per well, cultured in serum-free Dulbecco's modified Eagle's medium for 1 h, fixed in 4% paraformaldehyde, and viewed through a phase-contrast microscope (Nikon, Tokyo, Japan) to calculate the ratio of fully spreading cells to all cells observed in five randomly selected fields. HSFs were also cultured on the 96-well tissue culture plate coated with 10 μg/mL of the α1(I) chain as above to observe the cell morphology.

Culture of Cynomolgus Monkey Embryonic Stem (ES) Cells on Dishes Coated With the Recombinant α1(I) Chain

Cynomolgus monkey ES cells were cultured on murine embryonic fibroblast (MEF) feeder cells in Petri dishes (90 mm in diameter) according to previously established protocols (Cameron et al., 2006). Briefly, dishes were coated with the recombinant α1(I) chain by incubation with a solution of 1 mg/mL α1(I) chain for 30 min at room temperature. γ-Irradiated MEF cells were then cultured on the coated dishes as feeder cells for 1 day. Subsequently, monkey ES cells were seeded on MEF feeder layers and maintained by changing the medium. Immunostaining of monkey ES cell colonies was performed using NANOG, TRA1-81, SSEA-4, SOX2, and OCT4-specific primary antibodies (Millipore) according to the manufacturer's protocol. Nuclei were visualized by DAPI staining (Lin et al., 1976).

Monkey ES cells were injected subcutaneously into the hind leg of severe combined immunodeficient (SCID) mice (Suemori et al., 2001). Two months after injection, the mice were killed to remove teratomas. The teratomas

were then fixed with 4% paraformaldehyde in PBS, paraffin-embedded, sectioned, and histologically analyzed following staining with hematoxylin and eosin.

Results

Generation of Transgenic Silkworms

COL1A1/pMSG was injected into 9,834 pre-blastoderm embryos, and the hatched 5,282 G_0 larvae were allowed to develop to moths. G_1 embryos from the G_0 moths were screened for MGFP expression in the eyes and nervous tissues to obtain transgenic silkworms. Genomic Southern blot analysis of the transgenic silkworms demonstrated the existence of 41 independent transgenic lines with respect to the chromosomal insertion positions and copy numbers of the transgenes. Among them, 34 lines of transgenic silkworms with a single-copy transgene were selected, and the cocoon proteins of the lines were analyzed by SDS–PAGE. The line with the highest level of α1(I) chain expression was crossed with wild-type silkworms, and offspring hemizygous for the α1(I) chain gene were used in the following experiments as the COL249 line.

The worms of the COL249 line spun cocoons that were normal in appearance, size, and weight. Proteins in the sericin layer of the silk fibers of COL249 and wild-type silkworms were separated by SDS–PAGE and stained with CBB (Fig. 2, lanes 1–2). A band with an apparent molecular weight of 120 kDa was seen only in the cocoon proteins of COL249 (Fig. 2, lane 1). This band reacted with antihuman/bovine type I collagen antibody (Fig. 2, lane 6), indicating that this was the recombinant product from the human α1(I) chain gene. The band intensity of the recombinant α1(I) chain on the CBB-stained gel was quantified by densitometry. The content of the α1(I) chain was estimated to be 0.8% of the dried cocoon.

To increase the α1(I) chain content in the cocoon, a COL249 moth was crossed with an IM1 moth bearing the gene of the baculovirus-derived trans-activator IE1. Approximately 25% of the offspring carried both the α1(I) chain and IE1 genes hemizygously. The α1(I) chain/IE1 hemizygous silkworms (COL249/IM1) were further crossed with each other and silkworms homozygous for both the α1(I) chain and IE1 genes $(COL249/IM)^2$ were screened from the offspring by genomic PCR. Proteins in the cocoon extracts of COL249, COL249/IM, and $(COL249/IM)^2$ were separated by SDS–PAGE and stained with CBB (Fig. 3). By measuring the band intensity, the contents of the α1(I) chain in cocoons of the silkworm lines COL249, COL249/IM, and $(COL249/IM)^2$ were estimated to be 0.8%, 4.8%, and 8.0%, respectively. The average weights of cocoons in the COL249, COL249/IM, and $(COL249/IM)^2$ lines were 72, 65, and 53 mg, respectively. Although the cocoon weight decreased slightly with increased transgene copy numbers, the synthesis of the recombinant α1(I) chain per larvae was improved by this procedure; the amounts of the chain per cocoon of the COL249, COL249/IM, and $(COL249/IM)^2$ lines were 0.58, 3.12, and 4.24 mg, respectively.

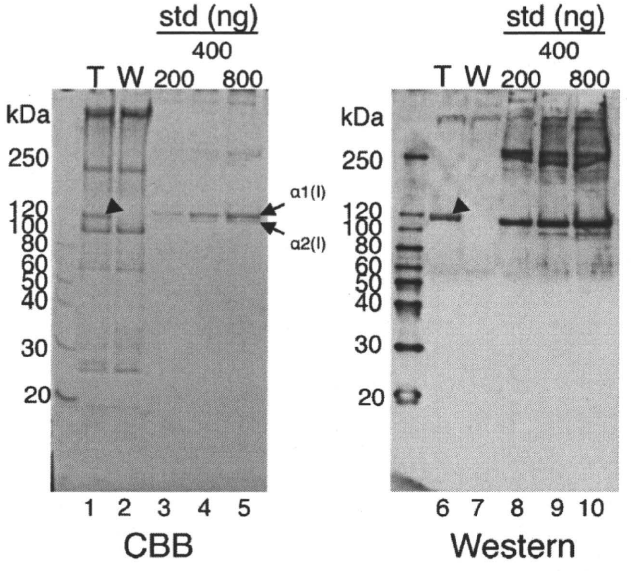

Figure 2. Expression of the α1(I) chain in cocoons of transgenic silkworms. The proteins in the cocoons of COL249 (T) and wild-type (W) silkworms were extracted with 8 M urea, 2% 2-mercaptoethanol, and 50 mM Tris–HCl, pH 8.0, separated by SDS–PAGE, and stained with CBB (**left panel**). Aliquots of the cocoon extracts were also assessed by Western blotting with antihuman/bovine type I collagen antibodies (**right panel**). Bovine pepsinized type I collagen in the amounts indicated was analyzed by CBB staining and Western blotting as a standard (std). The arrowheads in lanes 1 and 6 point to the band of the recombinant α1(I) chain. The arrows in lane 5 point to α1(I) and α2(I) chains of bovine type I collagen. Arabic numerals at the left side are molecular masses in kDa.

Extraction and Purification of the Recombinant α1(I) Chain From Cocoons

The extraction efficiency of the recombinant α1(I) chain from cocoons was examined. The powder of $(COL249/IM)^2$ cocoons was suspended in either PBS (Fig. 4A, lane 3), 0.5 M CH_3COOH, pH 3.0 (Fig. 4A, lane 4), 0.5 M CH_3COOH, pH 2.0 (Fig. 4A, lane 5), or 8 M urea and 0.5 M CH_3COOH, pH 2.0 (Fig. 4A, lane 6), at 4°C for 16 h, and the extracted proteins were analyzed by SDS–PAGE. Total proteins in the sericin layer of silk fibers of wild-type and transgenic silkworms were extracted by incubating cocoons at 80°C for 5 min in a buffer consisting of 8 M urea, 2% 2-mercaptoethanol, and 50 mM Tris–HCl, pH 8.0 (Fig. 4A, lanes 1 and 2). The ratios of the α1(I) chain extracted with the solutions to the total α1(I) chain in the sericin layer were calculated by quantifying the band intensities of the CBB-stained α1(I) chain. The efficiency of extraction was estimated to be 10% for PBS, 30% for 0.5 M CH_3COOH, pH 3.0, 50% for 0.5 M CH_3COOH, pH 2.0, and 80% for 8 M urea and 0.5 M CH_3COOH, pH 2.0. Thus, the use of CH_3COOH-solutions was more effective than PBS for extracting the recombinant α1(I) chain from

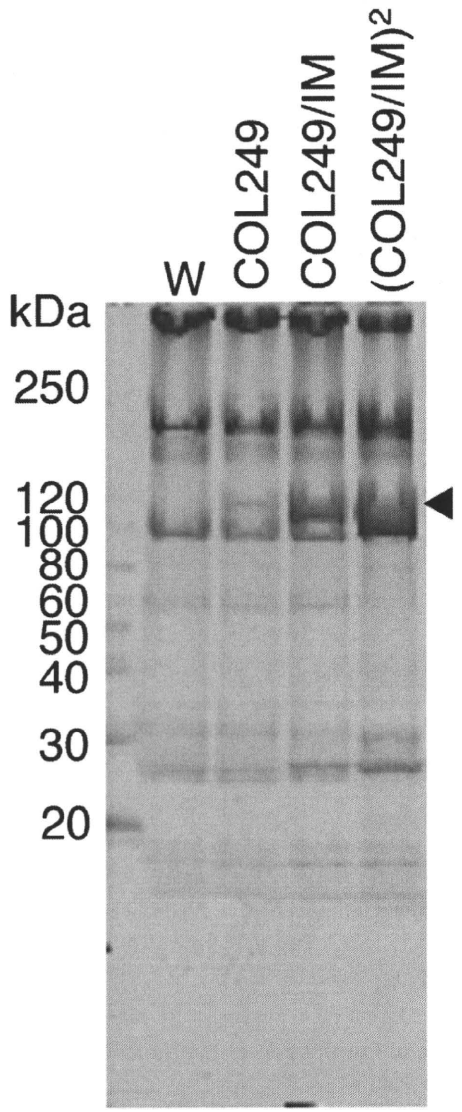

Figure 3. Increase in the α1(I) chain content in cocoons of transgenic silkworms. Transgenic silkworms were genetically modified to increase the amount of the α1(I) chain. Proteins were extracted from cocoons produced by wild-type (W), COL249, COL249/IM, and $(COL249/IM)^2$ silkworms, separated by SDS–PAGE, and stained with CBB. The arrowhead points to the band of the recombinant α1(I) chain. Arabic numerals at the left side are molecular masses in kDa.

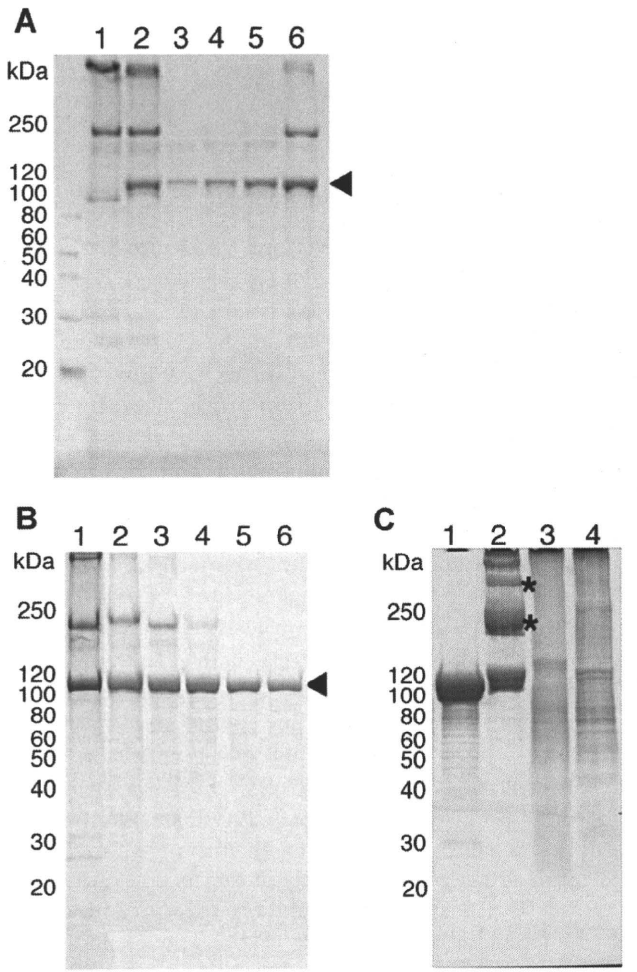

Figure 4. Extraction and purification of the α1(I) chain from cocoons of $(COL249/IM)^2$ silkworms. **A:** Extraction of the α1(I) chain from cocoons. Cocoon proteins were extracted with PBS (**lane 3**), 0.5 M CH_3COOH, pH 3.0 (**lane 4**), 0.5 M CH_3COOH, pH 2.0 (**lane 5**), and 8 M urea and 0.5 M CH_3COOH, pH 2.0 (**lane 6**). The extracted proteins were analyzed by SDS–PAGE. **Lanes 1** and **2** represent total proteins in the sericin layer of the silk fibers of wild-type and transgenic silkworms, respectively. The arrowhead points to the α1(I) chain. **B:** Analysis of the α1(I) chain in the purification processes. Cocoon proteins were extracted with 8 M urea and 0.5 M CH_3COOH, pH 2.0 (**lane 2**). The extracted proteins were concentrated by ultrafiltration (**lane 3**), and urea in the extract was removed by adding 0.5 M CH_3COOH, pH 2.0, and subsequent ultrafiltration (**lane 4**). After removing sericin by 0.5 M NaCl precipitation (**lane 5**), the α1(I) chain in the extract was collected by 4 M NaCl precipitation (**lane 6**). The proteins in each purification step were analyzed by SDS–PAGE and CBB staining. **Lane 1** represents total proteins in the sericin layer of the silk fibers. The arrowhead points to the α1(I) chain. **C:** Analysis of the purified α1(I) chain. Aliquots of 15 μg of proteins were electrophoresed and stained with CBB. **Lane 1**, the recombinant α1(I) chain; **lane 2**, bovine type I collagen; **lane 3**, alkaline-treated bovine gelatin; **lane 4**, acid-treated porcine gelatin. The asterisks in **lane 2** point to the dimer and trimer composed of the two and three α chains, respectively. Arabic numerals at the left side are molecular masses in kDa.

cocoons, and a major part of the α1(I) chain was extractive with 8 M urea and 0.5 M CH_3COOH, pH 2.0.

For purification of the α1(I) chain, 30 g of $(COL249/IM)^2$ cocoon powder, which was estimated to contain 2.4 g of the α1(I) chain, were suspended in 8 M urea and 0.5 M CH_3COOH, pH 2.0. The extracted α1(I) chain (Fig. 4B, lane 2) was concentrated by ultrafiltration (Fig. 4B, lane 3). The urea in the solution was removed by adding 0.5 M CH_3COOH, pH 2.0, and subsequent ultrafiltration. In this process, the endogenous sericin in the extract formed an insoluble aggregate, increasing the α1(I) chain content in the extract (Fig. 4B, lane 4). Small amounts of contaminated sericin were removed by 0.5 M NaCl precipitation (Fig. 4B, lane 5), and the α1(I) chain in the supernatant was then collected by precipitation with 4 M NaCl. The collected α1(I) chain was dissolved in 0.5 M CH_3COOH, pH 2.0, again, and the α1(I) chain solution was finally dialyzed against water (Fig. 4B, lane 6). The proteins in each

purification step and total proteins in the sericin layer (Fig. 4B, lane 1) were analyzed by SDS–PAGE, demonstrating that this simple purification process is sufficient to purify the α1(I) chain to apparent homogeneity. As a result, 990 mg of the α1(I) chain were purified from 30 g of cocoons; the recovery rate was estimated to be approximately 41%.

Biochemical Characterization

The purified recombinant α1(I) chain was analyzed by SDS–PAGE. Although small amounts of degradation products were found, the purified recombinant chain was composed of the polypeptide with a uniform molecular weight. The molecular weight of the chain was slightly smaller than the standard bovine α1(I) chain (Fig. 4C, lanes 1 and 2), indicating the possibility of insufficient prolyl-hydroxylation in the recombinant chain. The dimer (β chain) and trimer (γ chain) of the α chain, which were present in the standard collagen, were not detected from the purified recombinant chain, suggesting the absence of covalent cross-linking among the α1(I) chains. The molecular weight distribution of the recombinant α chain was quite different from that of the alkali-treated bovine (Fig. 4C, lane 3) or acid-treated porcine gelatins (Fig. 4C, lane 4). The gelatins gave broad molecular weight distributions because they were hydrolyzed products of collagens.

The α1(I) chain was subjected to an amino acid sequencer with five cycles of Edman degradation. The N-terminal amino acid sequencing of the α1(I) chain detected major and minor amino acid peaks in each cycle as shown in Table I. The sequence deduced from the minor peaks (GPM) was consistent with that of the predicted signal peptide cleavage (Fig. 1A) although peaks were not detected in the fourth and fifth cycles. The sequence from the major peaks (MGPSG) was probably derived from a cleavage at two amino acids downstream of the predicted site.

The amino acid composition of the purified α1(I) chain was determined after acid hydrolysis using a Hitachi L835 automated analyzer (Table II). The determined values were very similar to the predicted ones, except for the absence of hydroxyprolines and hydroxylysines.

The endotoxin levels of the α1(I) chain and the porcine gelatin were measured. The endotoxin level of the α1(I) chain was much lower (26 EU/g) than the gelatin (6,400 EU/g).

Structural Characterization

Far-ultraviolet (190–240 nm) CD spectra were recorded for the recombinant α1(I) chain, the native bovine type I collagen, the heat-denatured bovine type I collagen, and the porcine gelatin (Fig. 5A). The positive peak at 224 nm that is characteristic of the triple helical structure of collagen (Miller and Gay, 1982) was observed in the type I collagen. The gelatin exhibited a positive low peak at this wavelength, suggesting that the gelatin contained a partly formed triple helical structure in the molecule. In contrast, the recombinant α1(I) chain did not show a positive peak at 224 nm. The peak of the type I collagen disappeared when it was heat-denatured. The spectra of the denatured collagen were almost identical to those of the recombinant α1(I) chain. These results suggest that the α1(I) chain contained no triple helical structure. A negative peak at 198 nm represents the triple helical structure (Miller and Gay, 1982). The peak intensity at this wavelength of the recombinant α1(I) chain was similar to that of the heat-denatured collagen rather than that of gelatin, confirming the absence of the triple helical structure in the recombinant chain.

The 224-nm spectra were recorded for the recombinant chain, the native collagen, the denatured collagen and the gelatin at temperatures from 4 to 60°C (Fig. 5B). Apparent structural transition of the native collagen was observed in the range 39–46°C, which is in accordance with a report that the denatured temperature of bovine type I collagen is 42.8°C (Peltonen et al., 1980). In contrast, the recombinant α1(I) chain, the denatured collagen and the gelatin showed slight structural changes in the range 25–45°C.

The melting and gelation points of the 5% α1(I) chain or the gelatin solution were measured as described in the Materials and Methods Section. The melting and gelation

Table I. N-terminal sequencing.

Amino acid number	1	2	3	4	5
Major peaks	M	G	P	S	G
Minor peaks	G	P	M	—	—

Table II. Measurement of amino acid composition.

Amino Acid	Composition (mol%)	
	Recombinant α1(I) chain	Human α1(I) chain (predicted)
Aspartic acid	4.48	4.14
Threonine	1.56	1.58
Serine	2.91	3.35
Glutamic acid	7.71	7.30
Glycine	34.23	33.63
Alanine	11.72	11.74
Valine	1.81	1.87
Cystein	0.00	0.00
Methionine	0.33	0.69
Isoleucine	0.70	0.59
Leucine	2.12	1.87
Tyrosine	0.00	0.00
Phenylalanine	1.27	1.18
Hydroxylysine	0.00	2.37*
Lysine	3.66	1.18
Histidine	0.00	0.20
Arginine	4.71	5.03
Tryptophan	0.00	0.00
Hydroxyproline	0.00	11.44*
Proline	22.80	11.83
Total	100.00	100.00

*Assuming that all of lysine and proline residues in Y-position are hydroxylated.

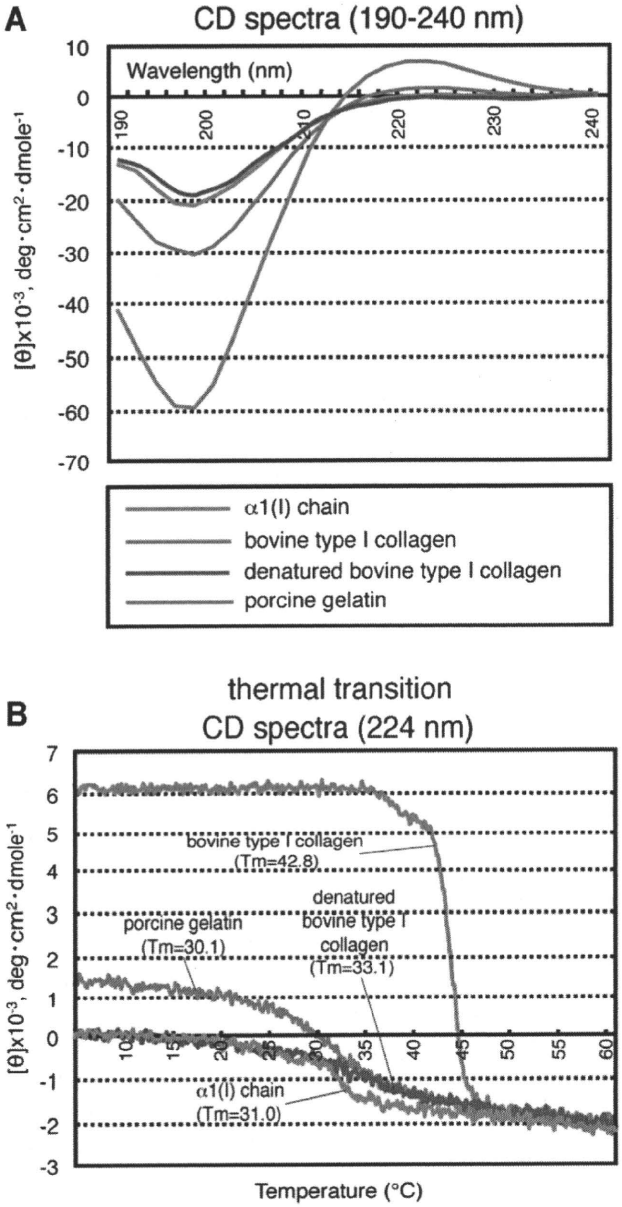

Figure 5. CD spectra of the α1(I) chain. **A:** Measurement of CD spectra of the α1(I) chain. Far-ultraviolet (190–240 nm) CD spectra were recorded for the recombinant α1(I) chain (red line), bovine type I collagen (pink line), denatured bovine type I collagen (blue line), and porcine gelatin (green line) at a concentration of 100 μg/mL. **B:** Thermal transition curves of the α1(I) chain. The CD spectra at 224 nm of the α1(I) chain, bovine type I collagen, denatured bovine type I collagen and porcine gelatin were monitored at temperatures from 4 to 60°C.

points of the α1(I) chain were 17 and 10°C, respectively, while the melting and gelation points of the gelatin were 30 and 26°C, respectively. Thus, both the melting and gelation points of the α1(I) chain were lower than the respective points of the gelatin, which may support the result from the measurement of CD spectra showing an absence of triple helical structures in the α1(I) chain. We also analyzed whether the α1(I) chain formed collagen fibrils under the physiological conditions as native collagen (Michalopoulos and Pitot, 1975) and found that the α1(I) chain did not form the fibrils (data not shown).

Cell Biological Properties

To investigate the cell biological properties of the recombinant α1(I) chain, HSFs were cultured on dishes coated with the α1(I) chain, the native collagen, or gelatin at various concentrations, and cell spreading on the materials was analyzed as described in the Materials and Methods Section (Fig. 6A). HSFs spread on all coating materials in a concentration-dependent manner. On collagen at concentrations of more than 0.63 μg/mL, HSFs spread at a rate of 100%. More than 80% of the cells spread on gelatin at concentrations >0.63 μg/mL, but 100% cell spreading was never observed even at the highest concentration tested (5.0 μg/mL). Cell spreading rates for the α1(I) chain at concentrations of <2.5 μg/mL were slightly low compared to those on gelatin at the same concentrations. However, HSFs spread on the α1(I) chain at a similar rate to on gelatin when inoculated at a concentration of 5.0 μg/mL. No differences were observed among cell morphologies when the cells were cultured on the α1(I) chain, the native collagen, or the gelatin at a concentration of 10 μg/mL (Fig. 6B, panels a–c). Cell-spreading was not observed on the uncoated dishes (Fig. 6B, panel d).

Cynomolgus monkey ES cells were cultured on feeder cells that had been cultured on dishes coated with the α1(I) chain or porcine gelatin. The ES cells cultured on dishes coated with the α1(I) chain formed tightly packed and flattened colonies (Fig. 7A, panel a). This morphology was the same as that of ES cell colonies cultured on dishes coated with porcine gelatin (Fig. 7A, panel b). Immunocytochemical studies confirmed that the monkey ES cell colonies on the α1(I) chain expressed the ES cell marker proteins NANOG, TRA1-81, SSEA-4, SOX2, and OCT4 (Fig. 7B). When the ES cells were subcutaneously injected into SCID mice after the passages on the α1(I) chain, the cells formed teratomas in the mouse tissues. Histological analyses of the teratomas showed formation of pigment epithelium, gastrointestinal epithelium, and cartilage (Fig. 7C). Thus, the α1(I) chain was confirmed to be useful for the maintenance of monkey ES cells.

Discussion

We generated transgenic silkworms that secreted the recombinant human α1(I) chain into the sericin layer of silk fibers. The content of the α1(I) chain in the cocoons of the established line COL249 was estimated to be 0.8%. By introducing the gene of the trans-activator IE1 into the silkworm as in our previous studies (Ogawa et al., 2007; Tomita et al., 2007), the expression of the α1(I) chain was enhanced to 4.8%. We then generated silkworms (COL249/

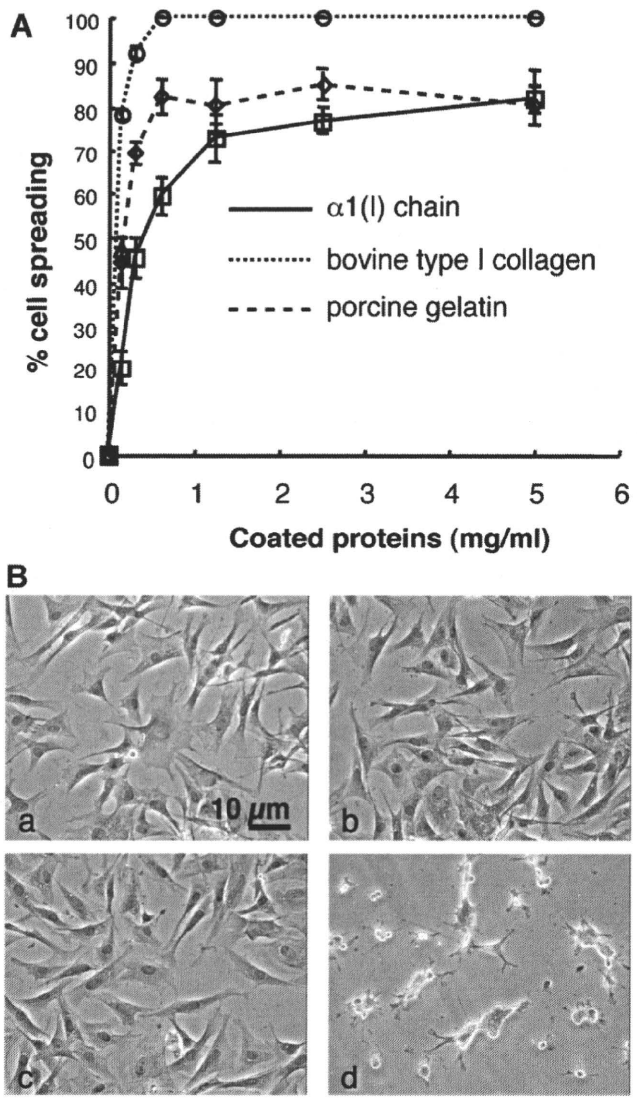

Figure 6. Spreading of HSFs on the α1(I) chain-coated dishes. **A**: Cell spreading assay using HSFs. The wells of tissue culture plates were coated with the α1(I) chain (black line), bovine type I collagen (dotted line), and porcine gelatin (dashed line) at various concentrations, and treated with heat-denatured bovine serum albumin to block the direct interaction between cells and the plate. HSFs were seeded on these wells and cultured for 1 h. The cells were then fixed, and the ratio of spreading cells to all cells in observed fields was calculated. **B**: Cell morphology of HSFs cultured on the α1(I) chain. HSFs were cultured on dishes coated with 10 μg/mL of the α1(I) chain (**a**), bovine type I collagen (**b**), porcine gelatin (**c**). The cells were also cultured on the uncoated but the albumin-treated dish (**d**). Scale bar, 10 μm.

IM)^2 homozygous for both the α1(I) chain and IE1 genes. This manipulation increased the α1(I) chain content up to 8.0%. Given that the average weight of a (COL249/IM)^2 cocoon was 53 mg, the α1(I) chain content per cocoon was calculated to be 4.24 mg. If 1,000 (COL249/IM)^2 silkworms were reared, we could produce 4.24 g of the α1(I) chain. The (COL249/IM1)^2 silkworm was generated from the pnd-w1 strain, which produces small cocoons (50–70 mg). Our preliminary experiment revealed that the cocoon weight could be increased to approximately 150 mg by crossing it with typical silkworm strains that produce 300- to 500-mg cocoons, leading to elevation of the α1(I) content to more than 10 mg per cocoon (data not shown). We also demonstrated the superiority of the transgenic silkworm system for the purification of the recombinant α1(I) chain. The α1(I) chain was highly purified from the cocoon extract by a simple method consisting of ultrafiltration and salt precipitation. Thus, this study offers experimental evidence for the viability of using transgenic silkworms in the production of the human recombinant α1(I) chain on an industrial scale.

Our previous study demonstrated that prolyl-hydroxylase activity is absent in silk glands (Adachi et al., 2005), and the recombinant fusion protein containing the collagen sequence expressed in the glands includes no hydroxyprolines (Tomita et al., 2005). The recombinant α1(I) chain produced in this study also contained no hydroxyprolines as predicted. The presence of hydroxyprolines is a prerequisite for forming the stable collagen triple helix (Berg and Prockop, 1973). In addition, the α1(I) chain did not contain the C-telopeptide and C-propeptide, which are known to promote triple helix formation (Doege and Fessler, 1986; Rosenbloom et al., 1976). Therefore, we postulated that the α1(I) chain is not capable of forming the triple helix. Indeed, CD spectra of the chain showed a complete absence of the triple helical structure. The importance of the telopeptide and propeptide for the triple helix formation was also shown in the previous studies. Unhydroxylated type I collagen with the telopeptide, and unhydroxylated α1(I) chain with the telopeptide and propeptide were synthesized as correctly folded triple helices in yeast (Olsen et al., 2001) and tobacco (Ruggiero et al., 2000), respectively. On the other hand, this study revealed that the animal-derived gelatin contained a partially folded triple helix, suggesting the significance of hydroxyprolines in the stability of triple helix. To further clarify the difference of physiological properties among the recombinant α1(I) chain, the gelatin and the collagen, we investigated the gelation and fibril-forming properties of the α1(I) chain. Unlike the collagen, the α1(I) chain did not form collagen fibrils under the physiological conditions examined. In contrast, the α1(I) chain, as well as the gelatin, gelated at lower temperatures than physiological ones. The melting and gelation points of the α1(I) chain were lower than those of gelatin. Thus, the physico-chemical properties of the recombinant α1(I) chain were similar to gelatin rather than collagen. However, due to the complete absence of the triple helical structure, the properties of the α1(I) chain differed slightly from those of gelatin.

The α1(I) chain promoted cell attachment and the spread of HSFs, but the cell-spreading rates for the α1(I) chain as well as gelatin were lower than those for collagen at all concentrations tested. At decreased concentrations of the materials, fewer cells spread on the α1(I) chain than on gelatin. Thus, HSFs were likely able to distinguish among these three materials. The cell–collagen interaction is mediated via integrins. Integrins α1β1 and α2β1 recognize collagens as collagen receptors (Hynes, 2002), and integrin

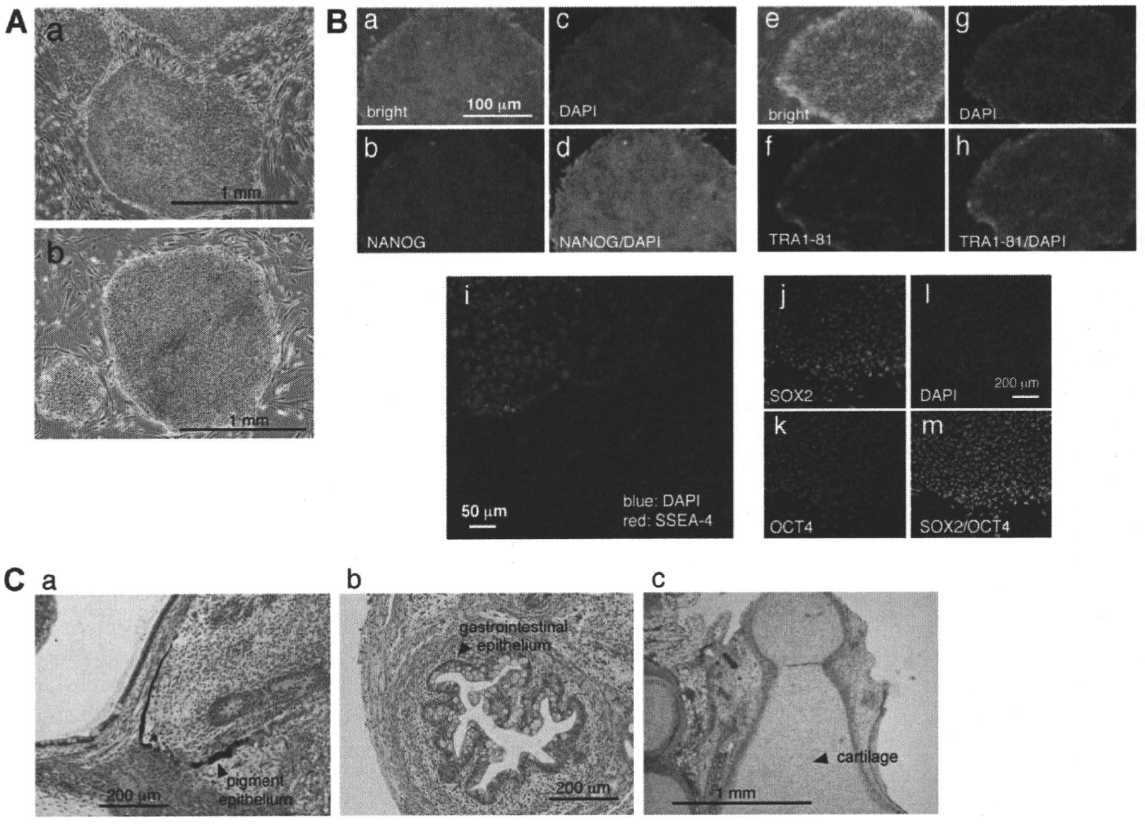

Figure 7. Culture of cynomolgus monkey ES cells on dishes coated with the α1(I) chain. **A**: Appearance of monkey ES cells. Cynomolgus monkey ES cells were cultured on feeder cells that had been cultured on dishes coated with the α1(I) chain (**a**) or porcine gelatin (**b**). Scale bar, 1 mm. **B**: Immunostain of the ES cell colonies. ES cell colonies were analyzed for the expression of marker proteins. **Panels (a–d** and **e–h)** show colonies immunostained with anti-NANOG and TRA1-81 antibodies, respectively. **Panels (a)** and **(e)**: appearances in bright fields; **panels (b)** and **(f)**: immunostained signals; **panels (c)** and **(g)**: DAPI-stained signals; **panels (d)** and **(h)**: mergers of immunostained and DAPI-stained signals. **Panel (i)** represents a colony stained with the anti-SSEA-4 antibody and DAPI. **Panels (j–m)** show a colony double-stained with anti-SOX2 and OCT4 antibodies. **Panel (j)**: immunostained signal with anti-SOX2 antibody; **panel (k)**: immunostained signal with anti-OCT4 antibody; **panel (l)**: DAPI-stained signal; **panel (m)**: merger of signals with anti-SOX2 and those with OCT4 antibodies. Scale bars, **(a)**: 100 μm; **(i)**: 50 μm; **(l)**: 200 μm. **C**: Teratoma formation in SCID mice. The ES cells were injected subcutaneously into the hind leg of SCID mice. Sections of the teratomas that formed were stained with hematoxylin and eosin. Arrowheads in **(a–c)** point to the pigment epithelium, gastrointestinal epithelium, and cartilage, respectively. Scale bars, **(a)** and **(b)**: 200 μm; **(c)**: 1 mm.

α5β1 indirectly recognizes it via collagen-bound fibronectin (Mould et al., 1997). Although the detailed mechanism is unknown, the complete absence of hydroxyprolines or the triple helical structure in the α1(I) chain may be responsible for this discrimination. At concentrations >5.0 μg/mL, however, HSFs spread on the α1(I) chain at a similar rate to that of gelatin. At a concentration of 10 μg/mL, the cell morphology was indistinguishable from that on collagen or gelatin. These results emphasize the practical utility of the recombinant α1(I) chain as a cell scaffold.

To demonstrate the practicality of the α1(I) chain, monkey ES cells were cultured on chain-coated dishes. After 30 passages, the monkey ES cell colonies maintained excellent morphology and the expression of several marker proteins for ES cells. The pluripotency of the cells was also confirmed by the formation of teratomas in SCID mice.

Gelatins are generally used for culturing ES or iPS cells. However, most marketed gelatins are derived from bovine or porcine bone, and therefore there is a risk of contamination with animal-derived pathogens, including viruses. In contrast, the recombinant α1(I) chain developed in this study does not pose such a risk because the chain is extracted from silk cocoons without using animal-derived materials. In addition, the α1(I) chain is composed of human sequences with constant molecular weight. Unlike the animal-derived gelatin extracted by hydrolyzing tissue collagens, the quality of the chain can be easily controlled with lot-to-lot consistency. The endotoxin level of the α1(I) chain was much lower than marketed gelatins. The recombinant α1(I) chain is a promising candidate material for use as a high-quality gelatin substitute for tissue engineering, drug delivery, and other applications.

References

Adachi T, Tomita M, Yoshizato K. 2005. Synthesis of prolyl 4-hydroxylase α subunit and type IV collagen in hemocytic granular cells of silkworm,

Bombyx mori: Involvement of type IV collagen in self-defense reaction and metamorphosis. Matrix Biol 24:136–154.

Adachi T, Tomita M, Shimizu K, Ogawa S, Yoshizato K. 2006. Generation of hybrid transgenic silkworms that express *Bombyx mori* prolyl-hydroxylase alpha-subunits and human collagens in posterior silk glands: Production of cocoons that contained collagens with hydroxylated proline residues. J Biotechnol 126:205–219.

Berg RA, Prockop DJ. 1973. The thermal transition of a non-hydroxylated form of collagen. Evidence for a role for hydroxyproline in stabilizing the triple-helix of collagen. Biochem Biophys Res Commun 52:115–120.

Bradley R. 1993. The research programme on transmissible spongiform encephalopathies in Britain with special reference to bovine spongiform encephalopathy. Dev Biol Stand 80:157–170.

Cameron CM, Hu WS, Kaufman DS. 2006. Improved development of human embryonic stem cell-derived embryoid bodies by stirred vessel cultivation. Biotechnol Bioeng 94:938–948.

Doege KJ, Fessler JH. 1986. Folding of carboxyl domain and assembly of procollagen I. J Biol Chem 261:8924–8935.

Fichard A, Tillet E, Delacoux F, Garron R, Ruggiero F. 1997. Human recombinant alpha1(V) collagen chain. Homotrimeric assembly and subsequent processing. J Biol Chem 272:30083–30087.

Garel A, Deleage G, Prudhomme JC. 1997. Structure and organization of the *Bombyx mori* sricin 1 gene and of the sericins 1 deduced from the sequence of the Ser 1B cDNA. Insect Biochem Mol Biol 27:469–477.

Geddis AE, Prockop DJ. 1993. Expression of human COL1A1 gene in stably transfected HT1080 cells: The production of a thermostable homotrimer of type I collagen in a recombinant system. Matrix 13:399–405.

Gill J, Feinberg J. 2001. Saquinavir soft gelatin capsule: A comparative safety review. Drug Saf 24:223–232.

Grzelak K. 1995. Control of expression of silk protein genes. Comp Biochem Physiol 110:671–681.

Hynes RO. 2002. Integrins: Bidirectional, allosteric signaling machines. Cell 110:673–687.

Iizuka M, Tomita M, Shimizu K, Kikuchi Y, Yoshizato K. 2008. Translational enhancement of recombinant protein synthesis in transgenic silkworms by a 5'-untranslated region of polyhedrin gene of *Bombyx mori* Nucleopolyhedrovirus. J Biosci Bioeng 105:595–603.

Iizuka M, Ogawa S, Takeuchi A, Nakakita S, Kubo Y, Miyawaki Y, Hirabayashi J, Tomita M. 2009. Production of a recombinant mouse monoclonal antibody in transgenic silkworm cocoons. FEBS J 276:5806–5820.

John DC, Watson R, Kind AJ, Scott AR, Kadler KE, Bulleid NJ. 1999. Expression of an engineered form of recombinant procollagen in mouse milk. Nat Biotechnol 17:385–389.

Lamberg A, Helaakoski T, Myllyharju J, Peltonen S, Notbohm H, Pihlajaniemi T, Kivirikko KI. 1996. Characterization of human type III collagen expressed in a baculovirus system. Production of a protein with a stable triple helix requires coexpression with the two types of recombinant prolyl 4-hydroxylase subunit. J Biol Chem 271:11988–11995.

Lee CH, Singla A, Lee Y. 2001. Biomedical applications of collagen. Int J Pharm 221:1–22.

Lin MS, Alfi OS, Donnell GN. 1976. Differential fluorescence of sister chromatids with 4'-6-diamidino-2-phenylindole. Can J Genet Cytol 18:545–547.

Merle C, Perret S, Lacour T, Jonval V, Hudaverdian S, Garrone R, Ruggiero F, Theisen M. 2002. Hydroxylated human homotrimeric collagen I in Agrobacterium tumefaciens-mediated transient expression and in transgenic tobacco plant. FEBS Lett 515:114–118.

Michalopoulos G, Pitot HC. 1975. Primary culture of parenchymal liver cells on collagen membranes. Morphological and biochemical observations. Exp Cell Res 94:70–78.

Miller EJ, Gay S. 1982. The collagens: An overview and update. Methods Enzymol 82:3–32.

Miyata T, Taira T, Noishiki Y. 1992. Collagen engineering for biomaterial use. Clin Mater 9:139–148.

Mould AP, Askari JA, Aota S, Yamada KM, Irie A, Takada Y, Mardon HJ, Humphries MJ. 1997. Defining the topology of integrin alpha5 beta1-fibronectin interactions using inhibitory anti-alpha5 and anti-beta1 monoclonal antibodies. Evidence that the synergy sequence of fibronectin is recognized by the amino-terminal repeats of the alpha5 subunit. J Biol Chem 272:17283–17292.

Mullins RJ, Richards C, Walker T. 1996. Allergic reactions to oral, surgical and topical bovine collagen. Anaphylactic risk for surgeons. Aust NZ J Ophthalmol 24:257–260.

Nicholls AC, Pope FM, Schloon H. 1979. Biochemical heterogeneity of osteogenesis imperfecta: New variant. Lancet 1:1193.

Ogawa S, Tomita M, Shimizu K, Yoshizato K. 2007. Generation of a transgenic silkworm that secretes recombinant proteins in the sericin layer of cocoon: Production of recombinant human serum albumin. J Biotechnol 128:531–544.

Olsen DR, Leigh SD, Chang R, McMullin H, Ong W, Tai E, Chisholm G, Birk DE, Berg RA, Hitzeman RA, Toman PD. 2001. Production of human type I collagen in yeast reveals unexpected new insights into the molecular assembly of collagen trimers. J Biol Chem 276:24038–24043.

Olsen D, Yang C, Bodo M, Chang R, Leigh S, Baez J, Carmichael D, Perala M, Hamalainen ER, Jarvinen M, Polarek J. 2003. Recombinant collagen and gelatin for drug delivery. Adv Drug Del Rev 55:1547–1567.

Peltonen L, Palotie A, Hayashi T, Prockop DJ. 1980. Thermal stability of type I and type III procollagens from normal human fibroblasts and from a patient with osteogenesis imperfecta. Proc Natl Acad Sci U S A 77:162–166.

Rosenbloom J, Endo R, Harsch M. 1976. Termination of procollagen chain synthesis by puromycin. Evidence that assembly and secretion require a COOH-terminal extension. J Biol Chem 251:2070–2076.

Ruggiero F, Exposito JY, Bournat P, Gruber V, Perret S, Comte J, Olagnier B, Garrone R, Theisen M. 2000. Triple helix assembly and processing of human collagen produced in transgenic tobacco plants. FEBS Lett 469:132–136.

Suemori H, Tada T, Torii R, Hosoi Y, Kobayashi K, Imahie H, Kondo Y, Iritani A, Nakatsuji N. 2001. Establishment of embryonic stem cell lines from cynomolgus monkey blastocysts produced by IVF or ICSI. Dev Dyn 222:273–279.

Tabata Y, Ikada Y. 1998. Protein release from gelatin matrices. Adv Drug Deliv Rev 31:287–301.

Tamura T, Thibert C, Royer C, Kanda T, Abraham E, Kamba M, Komoto N, Thomas JL, Mauchamp B, Chavancy G, Shirk P, Fraser M, Prudhomme JC, Couble P. 2000. Germline transformation of the silkworm *Bombyx mori* L. using a *piggyBac* transposon-derived vector. Nat Biotechnol 18:81–84.

Tomita M, Munetsuna T, Adachi T, Hino R, Hayashi M, Shimizu K, Nakamura N, Tamura T, Yoshizato K. 2003. Transgenic silkworms produce recombinant human type III procollagen in cocoons. Nat Biotechnol 21:52–56.

Tomita M, Shimizu K, Yoshizato K. 2005. Transgenic silkworms that weave recombinant human collagen in cocoons. In: Yoshizato K, editor. Transgenic silkworms: Eurekah Bioscience Collection. Georgetown: Landes Bioscience. chapter 2657.

Tomita M, Hino R, Ogawa S, Iizuka M, Adachi T, Shimizu K, Sotoshiro H, Yoshizato K. 2007. A germline transgenic silkworm that secretes recombinant proteins in the sericin layer of cocoon. Transgenic Res 16:449–465.

Vuorela A, Myllyharju J, Nissi R, Pihlajaniemi T, Kivirikko KI. 1997. Assembly of human prolyl 4-hydroxylase and type III collagen in the yeast *Pichia pastoris*: Formation of a stable enzyme tetramer requires coexpression with collagen and assembly of a stable collagen requires coexpression with prolyl 4-hydroxylase. EMBO J 16:6702–6712.

Werten MW, van den Bosch TJ, Wind RD, Mooibroek H, de Wolf FA. 1999. High-yield secretion of recombinant gelatins by *Pichia pastoris*. Yeast 15:1087–1096.

Yamada KM, Kennedy DW. 1984. Dualistic nature of adhesion protein function: Fibronectin and its biologically active peptide fragments can autoinhibit fibronectin function. J Cell Biol 99:29–36.

The American Journal of Pathology, Vol. 176, No. 4, April 2010

DOI: 10.2353/ajpath.2010.090486

Tumorigenesis and Neoplastic Progression

Function of *EWS-POU5F1* in Sarcomagenesis and Tumor Cell Maintenance

Takashi Fujino,*† Kimie Nomura,‡ Yuichi Ishikawa,‡ Hatsune Makino,§ Akihiro Umezawa,§ Hiroyuki Aburatani,¶ Koichi Nagasaki,‖ and Takuro Nakamura*

From the Divisions of Carcinogenesis, and Pathology,‡ and the Genome Center,‖ The Cancer Institute, Japanese Foundation for Cancer Research, Tokyo; the Department of Pathology,† Faculty of Medicine, Kyorin University, Tokyo; the Department of Reproductive Biology,§ National Institute for Child and Health Development, Tokyo; and the Genome Research Division,¶ Research Center for Advanced Science and Technology, University of Tokyo, Tokyo, Japan*

POU5F1 is a transcription factor essential for the self-renewal activity and pluripotency of embryonic stem cells and germ cells. We have previously reported that *POU5F1* is fused to *EWSR1* in a case of undifferentiated sarcoma with chromosomal translocation t(6;22)(p21;q12). In addition, the *EWS-POU5F1* chimeras have been recently identified in human neoplasms of the skin and salivary glands. To clarify the roles of the *EWS-POU5F1* chimera in tumorigenesis and tumor cell maintenance, we used small-interfering RNA-mediated gene silencing. Knockdown of *EWS-POU5F1* in the t(6;22) sarcoma-derived GBS6 cell line resulted in a significant decrease of cell proliferation because of G1 cell cycle arrest associated with $p27^{Kip1}$ up-regulation. Moreover, senescence-like morphological changes accompanied by actin polymerization were observed. In contrast, *EWS-POU5F1* down-regulation markedly increased the cell migration and invasion as well as activation of metalloproteinase 2 and metalloproteinase 14. The results indicate that the proliferative activity of cancer cells and cell motility are discrete processes in multistep carcinogenesis. These findings reveal the functional role of the sarcoma-related chimeric protein as well as POU5F1 in the development and progression of human neoplasms. *(Am J Pathol 2010, 176:1973–1982; DOI: 10.2353/ajpath.2010.090486)*

POU5F1/OCT4 is an essential transcription factor for the formation and/or maintenance of the inner cell mass of the mammalian blastocyst, the origin of pluripotent embryonic stem (ES) cells.[1–3] Suppression of *POU5F1* expression converts ES cells to trophoblasts, whereas overexpression of *POU5F1* leads to differentiation toward endoderm and mesoderm.[3,4] The self-renewal activity and pluripotency of ES cells are suppressed by knockdown of *POU5F1*.[5] These data suggest that POU5F1 orchestrates target gene expression in a tightly regulated manner during development and cellular differentiation. Also, POU5F1 induces reprogramming of somatic cells into iPS cells in combination with Sox2, c-Myc, and Klf4.[6] Moreover, two factors, either POU5F1 and Klf4 or POU5F1 and c-Myc, are apparently sufficient to generate iPS cells.[7]

In carcinogenesis, up-regulated expression of *POU5F1* is significantly correlated to certain lineages of human malignancies including germ cell tumors and breast and bladder cancer.[8–11] Reactivation of POU5F1 in somatic cells may induce dedifferentiation and may disrupt homeostasis, resulting in malignant transformation. Direct involvement of POU5F1 has been detected in a case of undifferentiated bone sarcoma with t(6;22)(p21;q12) translocation in which *POU5F1* is fused to *EWSR1*.[12] The chimeric *EWS-POU5F1* protein is composed of a transactivation domain of EWS and the entire DNA-binding domain of POU5F1. Ectopic overexpression of the POU5F1 component is achieved by the strong promoter activity of *EWSR1*.[12] Similar gene fusions between *EWSR1* and *POU5F1* have been identified in hidradenoma of the skin and mucoepidermoid carcinoma of the salivary glands.[13] These results underscore the important role of dysregulated *POU5F1* expression in human cancer and the important contributions of *EWS-POU5F1* to the development and maintenance of cancer cells.

In this study, we knocked down *EWS-POU5F1* by using *POU5F1*-specific small-interfering RNAs (siRNAs) in

Supported in part by Grant-in-Aid for Scientific Research on Priority Areas "Integrative Research Toward the Conquest of Cancer" from the Ministry of Education, Culture, Sports, Science, and Technology of Japan, and supported by Kawano Masanori Memorial Foundation for Promotion of Pediatrics.

Accepted for publication December 15, 2009.

Supplemental material for this article can be found on *http://ajp.amjpathol.org*.

Address reprint requests to Takuro Nakamura, M.D., Ph.D., Division of Carcinogenesis, The Cancer Institute, Japanese Foundation for Cancer Research, 3-8-31 Ariake, Koto-ku, Tokyo 135-8550, Japan. E-mail: takuro-ind@umin.net.

the GBS6 cell line established from the t(6;22) undifferentiated sarcoma.[12] Cellular growth was significantly suppressed by *EWS-POU5F1* depletion and was accompanied by up-regulation of $p27^{Kip1}$ expression, and senescence-like morphological alterations were observed. On the other hand, cell motility and invasive capacity were dramatically increased, and promotion of actin polymerization and activation of metalloproteinase (MMP)14 and MMP2 were observed. These results suggest that EWS-POU5F1 promotes proliferation of cancer cells but is dispensable for or even inhibits cell motility and invasiveness. This study provides important insights into EWS-POU5F1 function in carcinogenesis and tumor cell maintenance.

Materials and Methods

Cell Culture

The GBS6 cell line was established from a pelvic bone undifferentiated sarcoma with t(6;22)(p21;q12).[12] The cells were maintained at 37°C under 5% CO_2 in RPMI 1640 medium supplemented with 10% fetal bovine serum and 10 mmol/L of HEPES buffer, pH7.4. NIH3T3, HeLa, and HCT116 cells were grown at 37°C under 5% CO_2 in Dulbecco's modified Eagle's medium supplemented with 10% fetal bovine serum.

RNA Interference and DNA Transfection

RNA interference and DNA transfection experiments were performed by using Lipofectamine 2000 (Invitrogen, Carlsbad, CA). GBS6 cells were seeded on 12-well plates 24 hours before transfection at a density of 1×10^5 or 2.5×10^5 cells per well for siRNAs or plasmid DNAs, respectively. GBS6 cells were then transfected with 60 pmol or 1.6 μg of siRNAs or plasmids, respectively. The following siRNAs were purchased from Qiagen (Hilden, Germany): siRNA-POU5F1-1 (SI00690389) and siRNA-POU5F1-2 (SI026617) and control (non-sil). A FLAG-tagged p27 expression plasmid was a kind gift from Dr. Kei-ichi Nakayama.

Senescence-Associated β-galactosidase Assay

Senescence-associated β-galactosidase was detected histochemically by using a Senescence Detection Kit (Biovision, Mountain View, CA) 4 days after transfection of siRNAs.

Western Blotting

Whole cell lysates were size-fractionated by SDS-polyacrylamide gel electrophoresis and were transferred onto a nitrocellulose membrane. The membrane was blocked with Tris-buffered saline (pH 7.5) containing 0.2% Tween 20 and 5% nonfat dry milk. Primary antibodies used were as follows: goat anti-Oct3/4 (1:500 dilution; C-20, Santa Cruz Biotechnology, Santa Cruz, CA), mouse anti-lamin A/C (1:500 dilution; Santa Cruz Biotechnology), rabbit anti-p27 (1:200 dilution; Santa Cruz Biotechnology), mouse anti-p53 (1:200 dilution; DO-1, Santa Cruz Biotechnology), mouse anti-p21 (1:100 dilution; BD Biosciences, San Diego, CA), mouse anti-Rb (1:500 dilution; IF8, Santa Cruz Biotechnology), rabbit anti-Phospho-Rb (Ser807/811; 1:500 dilution; Cell Signaling Technology, Beverly, MA), mouse anti-cyclin D1 (1:500 dilution; A-12, Santa Cruz Biotechnology), rabbit anti-CDK2 (1:500 dilution; M2, Santa Cruz Biotechnology), rabbit anti-CDK4 (1:500 dilution; H-22, Santa Cruz Biotechnology), rabbit anti-CDK6 (1:500 dilution; C-21, Santa Cruz Biotechnology), mouse anti-MMP14 (1:200 dilution; Daiichi Fine Chemical, Tokyo, Japan), and mouse anti-RhoA (1:200 dilution; Upstate Biotechnology, Temecula, CA). The signals were detected by using appropriate secondary antibodies and an enhanced chemiluminescence kit (GE Health care, Piscataway, NJ).

Flow Cytometric Analysis

Single cell suspensions were permeabilized with 0.1% triton X-100 in PBS, and 50 mg/ml of propidium iodide and 1 mg/ml of RNase A were added. The cell suspensions were then analyzed by using a FACS-calibur flow cytometer (Beckton Dickinson, Franklin Lakes, NJ) and Modifit software (Beckton Dickinson).

Cell Invasion and Migration Assays

A quantitative invasion assay was performed by using a BD BioCoat Matrigel invasion chamber with 8-μm pore size membranes (BD Biosciences) according to the manufacturer's instruction. Briefly, cells incubated with siRNAs or plasmid DNAs for 24 hours were trypsinized and resuspended at a density of 1×10^5 cells per 1 ml of RPMI without serum. Cells (5×10^5) were then loaded onto inserts of the upper chambers. RPMI with 10% fetal bovine serum was added to the lower chambers. After 24 hours of incubation, cells on the upper surface membranes were removed gently with a cotton swab. Cells on the lower surface were stained with Wright-Giemsa solutions and air-dried. Cell migration was also evaluated by using the same chambers without Matrigel by assessing the cell numbers within the lower chamber. The invading or migrating cells were counted, and images were obtained by using an Olympus BX41 microscope with a 20× objective (Olympus, Tokyo, Japan). For the wound healing assay, GBS6 cells were cultured for 48 hours after transfection of siRNAs to reach 90% confluence in 12-well plates. A linear scratch, 100 μm in width, was produced by using a plastic tip. Cells were incubated in growth medium for the indicated period. Images were photographed by using an Olympus IX70 phase contrast microscope. The distance of cell migration from the scratch line was measured in micrometers on the photographs.

Gelatin Zymography

Conditioned media from GBS6 cell cultures were harvested 48 hours after siRNA transfection, loaded on 10% gelatin gels (Invitrogen), and electrophoresed. The gels were stained with 0.25% Coomassie Blue and were destained in 5% acetic acid/10% methanol to visualize bands corresponding to the gelatinolytic activity.

Total RNA Extraction, Conventional RT-PCR, and Real-Time Quantitative RT-PCR

Total RNA extraction, reverse transcription, and RNA quantification were performed according to methods described previously.[14] Conventional RT-PCR was performed by using a Gene Amp 9700 thermal cycler (Applied Biosystems, Foster City, CA). We conducted 40 cycles of three-step PCR (95°C for 30 seconds, 55°C for 1 minute, and 72°C for 1 minute) for miR032-367 locus and 25 cycles of three-step PCR (95°C for 30 seconds, 60°C for 30 seconds, and 72°C for 30 seconds) for actin. The specific forward and reverse primers for optimal amplification were designed as follows: miR302-367 locus, 5′-GGGCTCCCTTCAACTTTAAC-3′ and 5′-ATTCTGTCATTGGCTTAACAATCCATCACC-3′; β-actin, 5′-AGGCATCCTCACCCTGAAGTACCC-3′ and 5′-GCCAGGTCCAGACGCAGG-3′. Real-time RT-PCR was performed by using a 7500 Fast Real-Time PCR System (Applied Biosystems) using the following parameters: 40 cycles of three-step PCR (95°C for 15 seconds, 60°C for 30 seconds, and 72°C for 30 seconds). The specific forward and reverse primers to produce approximately 60-bp amplicons for optimal amplification in real-time PCR were designed as follows: MMP2, 5′-CCGCAGTGACGGAAAGATGT-3′ and 5′-GCCCCACTTGCGGTCAT-3′; MMP14, 5′-CGAGAGGAAGGATGGCAAATT-3′ and 5′-AGGGACGCCTCATCAAACAC-3′; β-actin, 5′-TGGATCAGCAAGCAGGAGTATG-3′ and 5′-GCATTTGCGGTGGACGAT-3′; and miR302-367 locus, 5′-TTTGAGTGTGGTGGTTCCTACCT-3′ and 5′- AGCCAAGAACTGCACACAGTGT-3′.

Actin Staining

GBS6 cells were seeded onto four-chamber culture slides (BD Biosciences) at a density of 3000 cells per well 24 hours after transfection and were incubated for an additional 24 hours in growth medium. Cells were then fixed and stained with phalloidin-rhodamine (Invitrogen). Images were photographed by using a Leica DM6000B laser scanning microscope with a 40× objective (Leica Microsystems, Cambridge, UK).

RhoA Activity Assay

To confirm RhoA activation, the amount of RhoA-GTP bound to the Rhotekin Rho-binding domain (RBD) was determined by using the Rho Activation Assay Kit (Upstate Biotechnology). Forty-eight hours after transfection of siRNAs, whole cell lysates were incubated with Rhotekin RBD-agarose for 45 minutes at 4°C. After washing, agarose beads were resuspended in Laemmli sample buffer, boiled for 5 minutes, and subjected to immunoblotting with an anti-RhoA antibody.

Microarray

The oligonucleotide array Human Genome U133 Plus 2.0 (Affymetrix, Santa Clara, CA), composed of 38,500 human genes and expressed sequence tags, was hybridized with cRNA probes generated from GBS6 cells 4 days after siRNA transfection and was scanned according to the method previously described.[14] The data were deposited in a public database (*http://www.ncbi.nlm.nih.gov/geo*, accession number: GSE12320, last accessed November 5, 2009). Clustering analysis was performed by using dChip software (*http://biosun1.harvard.edu/complab/dchip/* last accessed October 14, 2009). The gene network was analyzed by Webgestalat (*http://bioinfo.vanderbilt.edu/webgestalt/* last accessed October 31, 2009).

Statistical Analysis

Results were evaluated statistically by using Student's *t*-test. A value of $P < 0.05$ was considered significant.

Results

EWS-POU5F1 *Knockdown Induces p27^{Kip1} Up-Regulation and G1 Arrest*

The GBS6 cell line was established from a t(6;22) undifferentiated sarcoma that expressed the chimeric *EWS-POU5F1* but not wild-type *POU5F1*.[12] To investigate the biological role of *EWS-POU5F1*, we knocked down *EWS-POU5F1* in GBS6 cells by RNA interference. Effective knockdown of *EWS-POU5F1* on 2 days after transfection was confirmed for two independent *POU5F1*-specific siRNAs (Figure 1A, 88.3% of reduction by siRNA-1 and 85.9% by siRNA-2). The effects of the two siRNAs were similar to each other in every experiment, and the results using siRNA-POU5F1-1 are exhibited subsequently as a representative.

Suppression of *EWS-POU5F1* in GBS6 cells was significantly inhibited proliferation, the cell numbers being 58% or 54% of those treated with a control siRNA on day 2 or day 4, respectively (Figure 1B). A terminal deoxynucleotidyl transferase-mediated dUTP nick-end labeling assay did not show an apparent increase of apoptotic cells during treatment with RNA interference (data not shown). This result suggests that the suppression of cell growth might be because of inhibition of the cell cycle. Flow cytometric analysis demonstrated that knockdown of *EWS-POU5F1* significantly decreased the S-phase population and increased the G1 fraction compared with the control (Figure 1C), indicating that cell growth of GBS6 was suppressed because of G1 arrest.

We next examined the expression of a series of cell cycle regulators. Increased expression of p27 was observed in GBS6 cells during *EWS-POU5F1* knockdown (Figure 1D, left). An RT-PCR experiment showed no significant decrease of *p27* mRNA during *EWS-POU5F1*

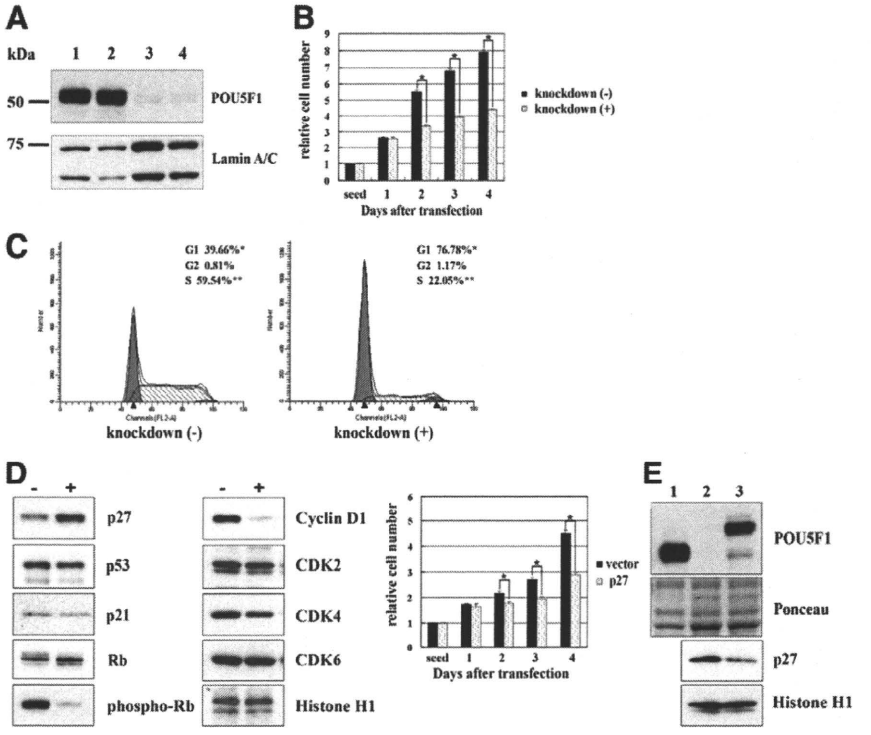

Figure 1. Knockdown of *EWS-POU5F1* inhibits proliferation of GBS6 cells accompanied by G1 cell cycle arrest and up-regulation of p27. **A:** RNA interference. GBS6 cells were transfected with control or *POU5F1* siRNAs and harvested 2 days after transfection; lysates were subjected to Western blotting by using anti-POU5F1 antibody. Lamin A/C was used as a control. **Lane 1**, wild-type; **lane 2**, negative control siRNA (non-sil); **lane 3**, POU5F1 siRNA-1; **lane 4**, POU5F1 siRNA-2. **B:** Proliferation assay of GBS6 cells treated with non-sil or POU5F1 siRNA. Mean of relative cell numbers ± SE of three independent experiments are presented ($^*P < 0.005$). **C:** Flow cytometric analysis of GBS6 cells treated with siRNAs. Average percentages of G1, G2, and S phases in three experiments are indicated. $^*P < 0.005$. **D:** Western blotting of GBS6 cells transfected with control (−) or POU5F1 (+) siRNAs by using antibodies specific for the indicated protein. Histone H1 was used as a loading control **(left)**; proliferation assay (**right**) of GBS6 cells in which p27 was introduced. Mean of relative cell numbers ± SE of three independent experiments are presented (*, $^{**}P < 0.005$). **E:** Western blotting of GBS6 cells and NIH3T3 cells transfected with an empty or *EWS-POU5F1* vectors by using anti-POU5F1 or anti-p27. **Lane 1**, GBS6 cells; **lane 2**, NIH3T3 treated with an empty vector; and **lane 3**, NIH3T3 treated with an *EWS-POU5F1* expression vector. Ponceau staining and Histone H1 were used as a loading control.

suppression (data not shown), suggesting that the change might be indirect and *p27* was not transcriptionally regulated by EWS-POU5F1. During knockdown, phosphorylation of Rb protein on Ser807/811 was significantly decreased, whereas expression of total Rb protein remained unchanged (Figure 1D, left). Expression of p21 and p53 was not affected (Figure 1D, left). In addition, a comparative genomic hybridization analysis revealed a homozygous loss of $p16^{INK4A}/p14^{ARF}$ (Supplemental Figure S1, see *http://ajp.amjpathol.org*). A significant decrease of cyclin D1 expression was also noted (Figure 1D, left). On the other hand, expression of CDK2, CDK4, and CDK6 was unchanged (Figure 1D, left).

Exogenous introduction of *p27* into GBS6 cells resulted in 82% and 61% decreased proliferation compared with the transfected controls on days 2 and 4, respectively (Figure 1D, right). Conversely, exogenous expression of *EWS-POU5F1* in NIH3T3 cells markedly depleted p27 (Figure 1E). However, expression of *EWS-POU5F1* did not affect proliferation of NIH3T3 cells, suggesting that the effect might be cell context-dependent. Taken together, these results indicate that EWS-POU5F1 supports tumor cell growth, at least in part, through down-regulating the $p27^{Kip1}$ activity.

Induction of the Senescence-Like Morphology by EWS-POU5F1 *Knockdown*

GBS6 cells possess a short spindle-shaped morphology with a narrow cytoplasm and a small nucleus with rough heterochromatin (Figure 2A, left), reflecting the original phenotype *in vivo*.[12] After introduction of *POU5F1*-specific siRNAs, we observed prompt enlargement of GBS6 cell bodies. Most GBS6 cells demonstrated large and flat cytoplasms as well as enlarged nuclei with fine chromatins 4 days after siRNA transfection. This morphology mimicked that observed in cellular senescence (Figure 2A, right). Most of the GBS6 cells enlarged by *EWS-POU5F1* knockdown expressed senescence-associated β-galactosidase (Figure 2B), a well-established biomarker of senescence.[15] However, senescence-associated heterochromatin foci, another biomarker of senescence,[16] were not observed (data not shown). Importantly, the enlarged GBS6 phenotype (and growth arrest) mediated by *POU5F1*-specific siRNAs disappeared 10 days after transfection when *EWS-POU5F1* expression returned (data not shown). Thus, the change was transient and reversible. These data suggest that the phenotypic changes were not because of senescence but rather indicated G1 arrest. Interestingly, overexpression of $p27^{Kip1}$ did not induce morphological changes in GBS6 cells (data not shown), indicating that different molecular pathways downstream of EWS-POU5F1 are responsible for the senescence-like morphologies.

Drastic modification of the cytoskeleton was also observed in siRNA-treated enlarged GBS6 cells. Phalloidin staining revealed prominent networks of F-actin throughout the cytoplasm of siRNA-treated cells (Figure 2C, right). Control GBS6 cells showed only a small amount of actin fibers in the cytoplasmic rim (Figure 2C, left). A close link between actin polymerization and a small G protein Rho has been reported.[17] Indeed, a GTP-bound activated form of RhoA protein was apparently increased on *EWS-POU5F1* knockdown (Figure 2D). These data indicate that EWS-POU5F1 affected the RhoA signaling pathway and morphology of tumor cells by modulating the actin fiber network. Finally, transfection of *POU5F1*-specific siRNA into HeLa cells that do not express *POU5F1* did not affect cell morphology (Figure 2E), indi-

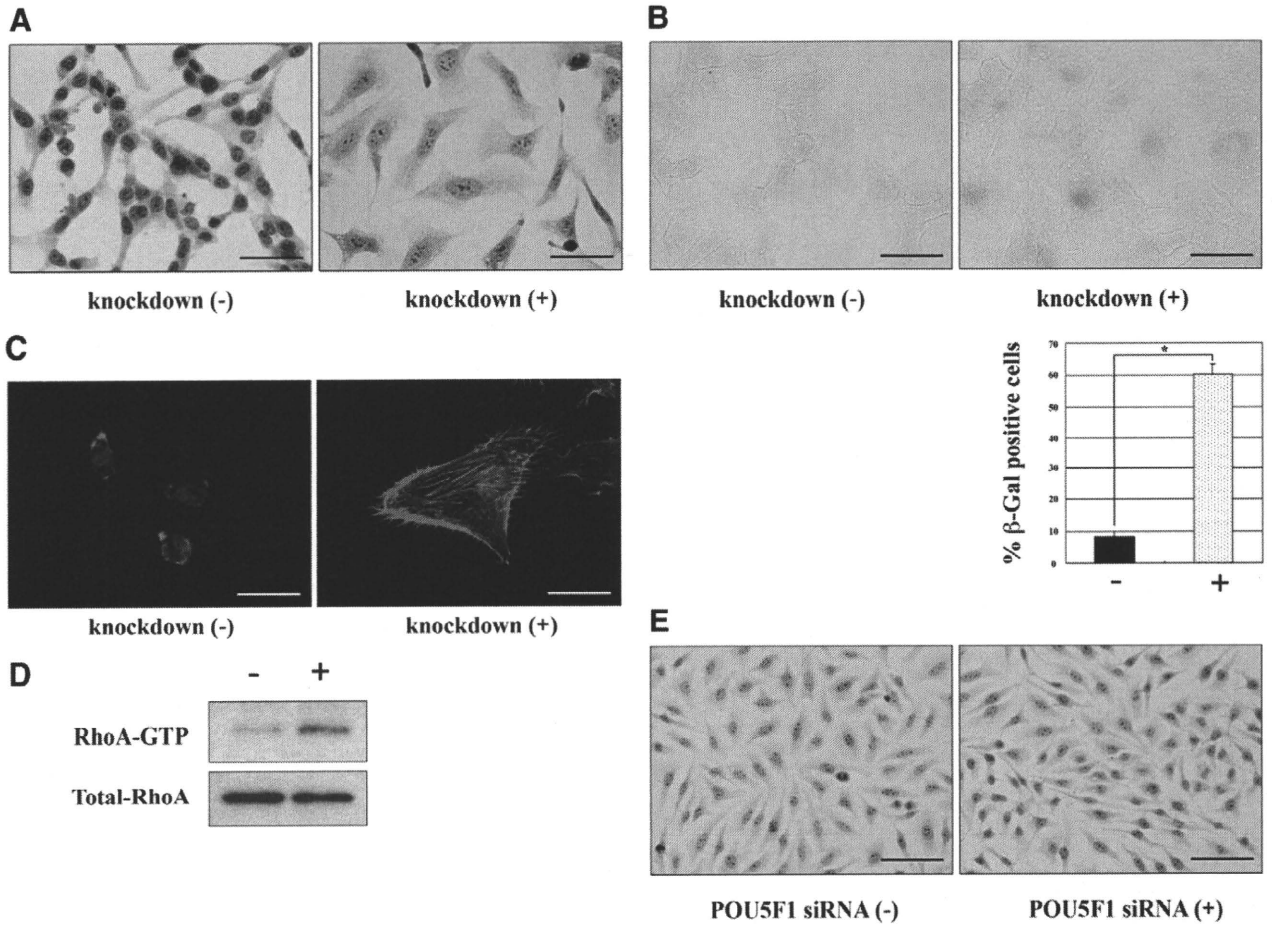

Figure 2. Morphological changes and actin polymerization in siRNA-treated GBS6 cells. **A:** Photomicrographs of GBS6 cells transfected with control siRNA or *POU5F1*-specific siRNA. Papanicolau staining, ×400 original magnification. Scale bars = 100 μm. **B:** Senescence-associated β-galactosidase (SA-β-Gal) assay 4 days after transfection of siRNAs. Original magnification, ×400. Scale bars = 100 μm. The columns indicate mean % SA-β-Gal-positive cells in three independent experiments (*$P < 0.005$). **C:** Enhanced actin polymerization in *EWS-POU5F1* silent GBS6 cells. F-actin was visualized by phalloidin-rhodamine staining. Original magnification, ×400. Scale bars = 100 μm. **D:** Increased RhoA-GTP in *EWS-POU5F1* silenced GBS6 cells (+) compared with control (−). **E:** *POU5F1* knockdown does not affect morphology of HeLa cells. Papanicolau staining, ×200 original magnification. Scale bars = 100 μm.

cating that the above findings are not because of non-specific effects of *POU5F1* siRNAs.

Knockdown of EWS-POU5F1 *Promotes Cell Migration and Invasion*

Uncontrolled proliferation and metastatic activities are important biological characteristics of cancer.[18] Indeed, in the t(6;22) sarcoma case, the patient died of multiple pulmonary metastases.[12] Therefore, it is intriguing to clarify whether EWS-POU5F1 promotes cell migration and invasiveness. Migration and invasion of GBS6 cells treated with siRNA for *EWS-POU5F1*were assessed in a Matrigel invasion assay. *EWS-POU5F1* knockdown resulted in marked increases in migration and invasion activities compared with the control GBS6 cells (Figure 3A and Table 1). The original GBS6 cells rarely migrated *in vitro*; however, the number of cells migrating in the absence of EWS-POU5F1 increased more than 50-fold. The increase in cell motility after *EWS-POU5F1* knockdown was also confirmed by a wound healing assay, showing that GBS6 cells with *EWS-POU5F1* knockdown migrated 2.5-fold faster than the control cells (Figure 3B).

We next asked whether the enhanced invasiveness of GBS6 cells in Matrigel was solely because of increased cell motility or whether invasiveness itself was also accelerated. Because cell invasion activity is closely associated with increased metalloproteinase activity,[19,20] MMP2 and MMP9 activities were assessed by gelatin zymography. The zymogram exhibited a significant increase of the gelatinolytic activity of MMP2, whereas the MMP9 activity was not altered (Figure 3C, top). MMP14/MT1-MMP, a membrane-type MMP, activates pro-MMP2 in collaboration with a tissue inhibitor of metalloproteinase 2.[19,21] An immunoblot analysis demonstrated increased expression of the MMP14 protein (Figure 3C, bottom), consistent with promotion of MMP2 activity. Thus, *EWS-POU5F1* knockdown increased cell motility and also enhanced invasiveness through accelerated degradation of matrix by MMPs.

Real-time quantitative RT-PCR showed that expression of MMP2 and MMP14 was also increased at the RNA level (Figure 3D), suggesting that *EWS-POU5F1* may also

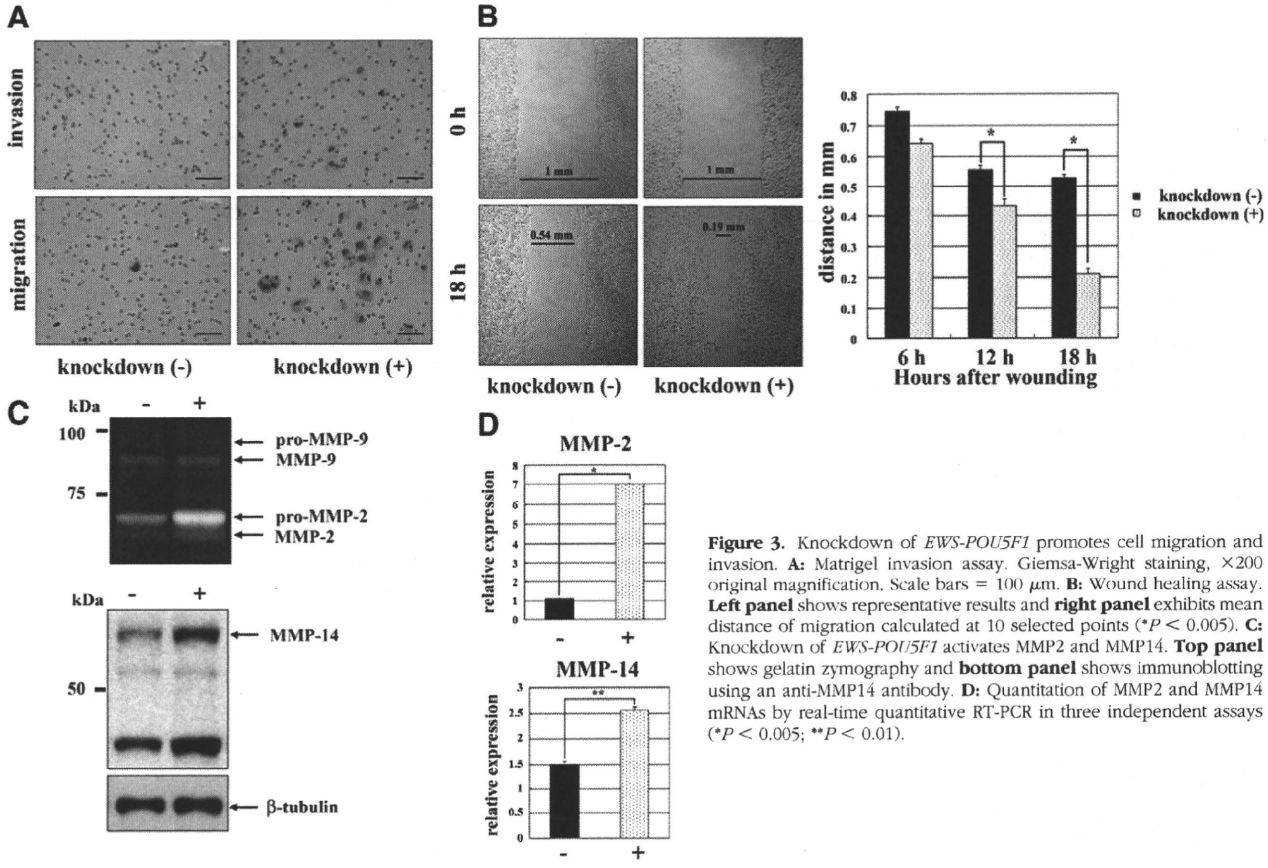

Figure 3. Knockdown of *EWS-POU5F1* promotes cell migration and invasion. **A:** Matrigel invasion assay. Giemsa-Wright staining, ×200 original magnification. Scale bars = 100 μm. **B:** Wound healing assay. **Left panel** shows representative results and **right panel** exhibits mean distance of migration calculated at 10 selected points (*$P < 0.005$). **C:** Knockdown of *EWS-POU5F1* activates MMP2 and MMP14. **Top panel** shows gelatin zymography and **bottom panel** shows immunoblotting using an anti-MMP14 antibody. **D:** Quantitation of MMP2 and MMP14 mRNAs by real-time quantitative RT-PCR in three independent assays (*$P < 0.005$; **$P < 0.01$).

regulate MMP expression directly or indirectly. The Matrigel invasion assay was also performed by using HeLa cells after introduction of the *EWS-POU5F1* expression vector. Cellular invasiveness was again suppressed (Figure 4A and Table 1; $P < 0.01$), though cell migration was decreased only moderately. In addition, depletion of MMP14 protein was demonstrated by introduction of *EWS-POU5F1* into both HeLa and HCT116 colon carcinoma cells (Figure 4B). Overexpression of *EWS-POU5F1* did not affect the expression level of p27, MMP2, or MMP9 in HeLa or HCT116 cells (data not shown). These results suggest that EWS-POU5F1 suppresses cellular motility and invasion in the broad cellular context. In contrast, overexpression of $p27^{Kip1}$ did not affect either cell migration or invasion (Table 1), clearly indicating that cell motility/invasiveness is modulated in a p27-independent manner in GBS6 cells and that simple growth suppression is not sufficient to enhance the invasive activity of tumor cells.

Modulation of the Gene Expression Profile by EWS-POU5F1 *Suppression*

To investigate important downstream molecules regulated by EWS-POU5F1, alteration of global gene expression profiles by *EWS-POU5F1* knockdown was examined. We compared RNAs derived from *POU5F1*-specific siRNA-treated and control GBS6 cells (4 days after siRNA treatment) by using 54,676 probe sets of Affymetrix GeneChip Human Genome U133 Plus 2.0. We identified 98 probe sets (80 genes), the expression of which was increased more than 1.5-fold, and 55 probe sets (45 genes), the expression of which was decreased more than 1.5-fold (Figure 5A and Supplemental Table S1 at *http://ajp.amjpathol.org*). The genes whose expression was modified significantly were then classified according to gene ontology categories (Figure 5B). Interestingly,

Table 1. Invasiveness and Migration of GBS6 and HeLa Cells

	EWS-POU5F1 knockdown in GBS6		*p27* expression in GBS6		*EWS-POU5F1* expression in HeLa	
Cells and treatment	−	+	−	+	−	+
No. invasion	0.3 ± 0.4	101 ± 19*	0	0	1108 ± 85	357 ± 64*
No. migration	9.3 ± 3.2	>500*	11.1 ± 1.1	3.0 ± 0.7	3628 ± 401	1725 ± 229

Mean values ± SE of cell numbers of invasion and migration per 5×10^5 cells are exhibited.
*$P < 0.01$ versus control (−).

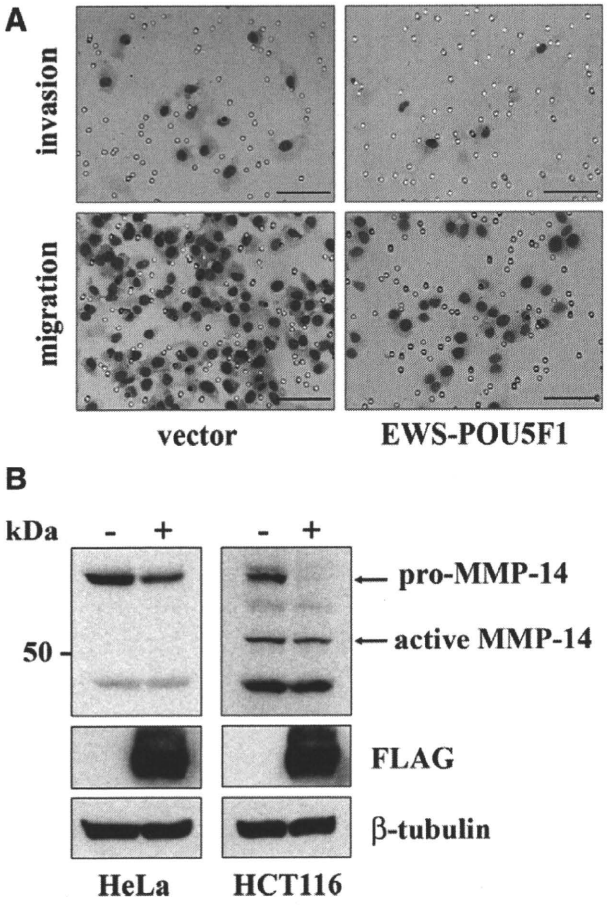

Figure 4. Inhibition of cell migration and invasion by EWS-POU5F1 in HeLa cells. **A:** Matrigel invasion assay. Giemsa-Wright staining, ×200 original magnification. Scale bars = 100 μm. **B:** Immunoblotting of HeLa cells transfected with control (−) or *EWS-POU5F1* (+) expression vectors using anti-MMP14 (**top**), anti-FLAG (**middle**), and anti-β-tubulin (**bottom**).

23.8% of up-regulated genes were involved in cell motility, invasion, or cytoskeleton, consistent with the remarkable alteration of the phenotypes in GBS6 cells. In addition, 13.3% of down-regulated and 13.8% of up-regulated genes belong to differentiation and development categories, indicating importance of the POU5F1 function in pluripotency. However, *EWS-POU5F1* knockdown did not induce GBS6 cells to differentiate toward any specific lineage.

Representative differentially expressed genes of interest belonging to motility, adhesion/invasiveness, morphology/cytoskeleton, mesodermal differentiation, and growth suppression categories are shown in Figure 5C. In motility and adhesion/invasiveness categories, up-regulation of *MMP2* was again observed, though *MT1-MMP* was up-regulated only marginally. We also noted up-regulation of *CAV1*, the mutation of which is associated with mammary carcinoma invasiveness.[22] In addition, another up-regulated gene, *F2R*, has been reported as overexpressed in human cancers with high metastatic potency.[23] Down-regulation of *ELMO1* is intriguing because it is required for promoting phagocytosis and cell shape changes.[24]

A number of genes involved in the differentiation process were up-regulated by *EWS-POU5F1* knockdown. *MGP*, *LBH*, *JUN*, *MYOF*, *CTGF*, and *MESDC2* are involved in mesodermal differentiation (Figure 5C and Supplemental Table S1 at *http://ajp.amjpathol.org*). The mesodermal origin of t(6;22) sarcoma was also supported by the fact that a number of genes encoding extracellular matrix proteins were also up-regulated. However, any specific differentiation toward muscle, bone, cartilage, or adipocytes was not supported by gene expression profiling.

Four putative tumor suppressors, *IGFBP7*, *HTRA1*, *TGFBR2*, and *SOCS3*, were up-regulated by *EWS-POU5F1* knockdown.[25–28] Although it remains unclear whether these genes are the direct targets of EWS-POU5F1, modified expression of these genes should be noted in addition to the altered state of p27, cyclin D1, and Rb. In summary, expression profiling provided important information on the molecular networks affected by the oncogenic function of EWS-POU5F1.

EWS-POU5F1 Up-Regulates the ES Cell-Specific miR302-367 Cluster

MicroRNAs (miRNAs) are noncoding RNAs consisting of approximately 22 nucleotides, which posttranscriptionally regulate mRNAs. They are important in development and differentiation, and abnormal expression of miRNAs has been reported in various neoplasms.[29,30] The miR302-367 cluster has been identified recently as ES cell-specific, and the cluster is transcriptionally regulated by Nanog, POU5F1, Sox2, and Rex1.[31,32] RT-PCR analysis revealed remarkable down-regulation of the miR302-367 cluster during knockdown of *EWS-POU5F1* (Figures 6A and 6B), suggesting that chimeric EWS-POU5F1, like wild-type POU5F1, may regulate miR302-367. The result strongly suggests that EWS-POU5F1 regulates downstream genes not only by its direct DNA binding but also through modulating the expression of miRNA.

Discussion

In the present study we show that EWS-POU5F1 enhances cellular proliferation of GBS6 sarcoma cells. Knockdown of *EWS-POU5F1* caused GBS6 cells to arrest in the G1 phase of the cell cycle. We also noted up-regulation of $p27^{Kip1}$, down-regulation of cyclin D1, and diminished phosphorylation of Rb protein. The tumor suppressor $p27^{Kip1}$ is a CDK2 inhibitor, and it inhibits the cell cycle at the G1/S transition.[33] It is likely that $p27^{Kip1}$ functions downstream from EWS-POU5F1 in oncogenic transformation. In support of this idea, exogenous introduction of $p27^{Kip1}$ blocked proliferation of GBS6 cells.

During suppression of *EWS-POU5F1*, GBS6 cells showed morphological changes similar to those seen in cellular senescence (eg, spreading of the cytoplasm, marked enlargement of cell size, and expression of senescence-associated β-galactosidase, a hallmark of senescence).[15] However, the lack of senescence-associated heterochromatin foci[16] and the reversible nature of the G1 arrest suggest that the change induced by *EWS-POU5F1* knockdown differs from senescence. Loss of $p16^{INK4A}$ might protect GBS6 cells from senescence,

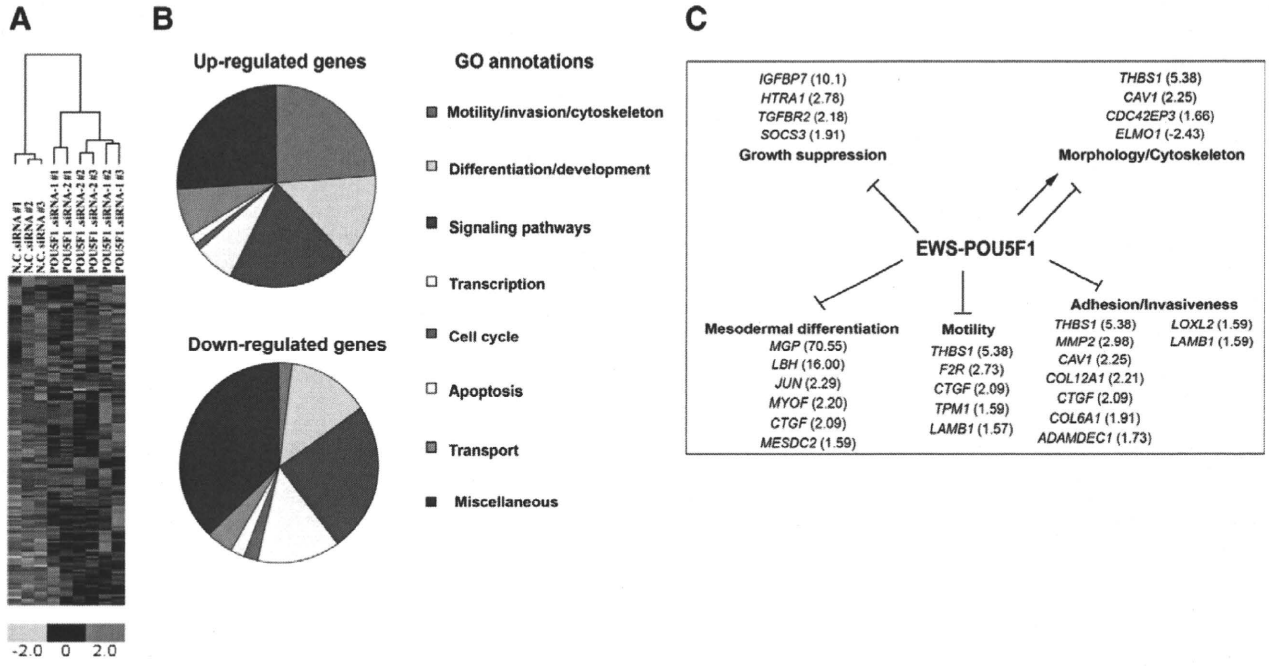

Figure 5. Gene clustering analysis across the compared populations. **A:** Heat map shows the expression of EWS-POU5F1 regulated genes in GBS6 cells treated with negative control siRNA or *POU5F1*-specific siRNAs. Up-regulated and down-regulated genes are presented in red and green, respectively. **B:** Pie charts show the distribution of the 80 up-regulated and 45 down-regulated genes in GBS6 cells transfected with *POU5F1* siRNAs according to gene ontology (GO) annotations. **C:** Prediction of the major signaling pathways affected by EWS-POU5F1. Lower bound of fold changes in each gene are indicated in parentheses.

and senescence-like morphological changes might be achieved by alteration of the actin fiber network.

The inhibitory role of EWS-POU5F1 in cell migration and invasion was unexpected. It is very likely that multiple molecular processes were responsible for increased motility and invasiveness of GBS6 cells treated with *POU5F1* siRNAs. It has been reported that RhoA activation induces actin polymerization[17] that is causatively related to cancer cell invasion and migration.[34] Paradoxical promotion of tumor invasiveness related to $p27^{Kip1}$-dependent G1 arrest has been reported in malignant melanoma with Mitf activation in which Mitf promotes melanoma proliferation by down-regulating $p27^{Kip1}$ but suppresses tumor cell invasion by the Dia1-dependent pathway.[35] Furthermore, $p27^{Kip1}$ supports cell motility through modulation of the RhoA pathway.[36] In GBS6 cells, however, introduction of $p27^{Kip1}$ affected neither cell mobility/invasiveness nor morphological changes. Those results suggest that there might be a $p27^{Kip1}$-independent pathway in RhoA activation and actin polymerization. MMP2 and MT1-MMP, which were up-regulated by knockdown of *EWS-POU5F1*, are candidate upstream regulators of RhoA because recent studies indicate these MMPs induce RhoA activation in osteosarcoma and vascular endothelial cells.[37,38] Moreover, our study indicates that increased cell motility was not a simple consequence of growth suppression. Furthermore, the present results raise an important concern for the treatment of cancer in general. That is, when treatment suppresses the expression of oncogenic transcription factors, inhibition of tumor growth might be accompanied by enhanced tumor cell invasion and metastasis.

Carcinogenesis is a multistep process that requires multiple genetic and epigenetic alterations.[39] Therefore, the fusion of *EWSR1* and *POU5F1* is not sufficient for complete carcinogenesis, and t(6;22) tumors possess additional mutations such as *p16/p14* loss. Our prelimi-

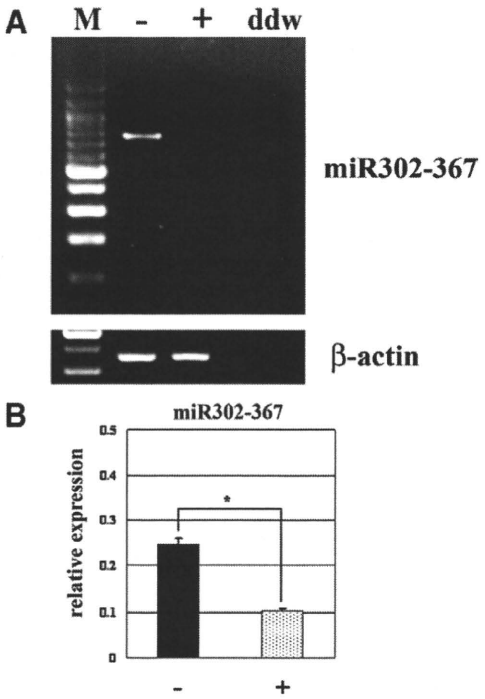

Figure 6. **A:** RT-PCR analysis of miR302-367 in GBS6 cells transfected with control (−) or POU5F1 (+). β-actin was amplified to confirm qualities and quantities of RNA. **B:** Real time quantitative RT-PCR analysis of miR302-367. Average expression was calculated in three independent experiments ($^*P < 0.005$).

nary study demonstrated that retrovirus-mediated gene transfer of *EWS-POU5F1* could immortalize but not induce full transformation of murine mesenchymal stem cells (M. Tanaka and T. Nakamura, unpublished observation). Identification of genes cooperative with *EWS-POU5F1* for carcinogenesis is important, and genetic analysis including mutagenesis experiments will provide useful information for understanding the mechanism of *POU5F1*-induced carcinogenesis. In addition, our study suggests that tumor progression toward invasive properties may be caused by genes that do not cooperate with *EWS-POU5F1* but may even counteract *EWS-POU5F1*.

It is intriguing to define important EWS-POU5F1 target genes in carcinogenesis. Because POU5F1/Oct3/4 is a transcriptional regulator, it is likely that the fusion to EWS modulates the nature of its regulatory activities for downstream target genes. Previous studies suggested that POU5F1 acquires the enhanced transcriptional activity by addition of the EWS N-terminal domain.[13,40] The target genes for POU5F1 have been extensively investigated by using ES cells.[4,41,42] In these studies POU5F1 is found associated with SOX2 and/or Nanog, both of which are also expressed in GBS6 cells (data not shown). However, the down-regulated genes in *EWS-POU5F1* knockdown GBS6 cells did not always overlap with POU5F1 target genes in ES cells, probably because of the different cellular context between ES cells and sarcoma cells. Alternatively, the addition of the EWS N-terminal domain may alter the binding specificity of POU5F1 to the target sequences. Nevertheless, it is still possible that there are common target genes for both EWS-POU5F1 and wild-type POU5F1. In a comparison between genes showing altered expression on *EWS-POU5F1* knockdown in the present study and the genes detected in chromatin immunoprecipitation (ChIP)-on-chip or chromatin immunoprecipitation-paired-end ditag (ChIP-PET) studies,[41,42] *INSIG1*, *EPHA4*, *DHCR7*, *ANKS1B*, *ANO4*, *RDH10*, *PHF19*, *BNIP3*, and *TRIB1* are good candidates for common target genes of POU5F1 or EWS-POU5F1 in organogenesis or sarcomagenesis. In addition, the miR302-367 cluster has been identified as a target of ES cell-associated transcription factors, including POU5F1.[32] Down-regulation of miR302-367 on *EWS-POU5F1* knockdown strongly suggests that EWS-POU5F1 regulates gene expression by recognition of a target sequence as well as miRNA-mediated mRNA inhibition. In fact, overexpression of miR302 induces cell cycle progression of ES cells.[43] Interestingly, miR302 represses protein expression of cyclin D1 in ES cells, the opposite effect for EWS-POU5F1 in GBS6 cells, suggesting cell context-dependent function of the miR302-467 cluster. Further studies are needed to identify key downstream molecules controlling cell proliferation and/or cell motility and invasiveness.

Acknowledgments

We thank Dr. Kei-ichi Nakayama for providing a human p27 expression vector, Dr. Eiji Hara and Dr. Akiko Takahashi for valuable discussion, and Ms. Sayuri Amino-Shibuya and Ms. Rie Furuya for technical assistance.

References

1. Schöler HR, Dressler GR, Balling R, Rohdewohld H, Gruss P: Oct-4: a germline-specific transcription factor mapping to the mouse t-complex. EMBO J 1990, 9:2185–2195
2. Nichols J, Zevnik B, Anastassiadis K, Niwa H, Klewe-Nebenius D, Chambers I, Schöler H, Smith A: Formation of pluripotent stem cells in the mammalian embryo depends on the POU transcription factor Oct4. Cell 1998, 95:379–391
3. Niwa H, Miyazaki J, Smith AG: Quantitative expression of Oct-3/4 defines differentiation, dedifferentiation or self-renewal of ES cells. Nat Genet 2000, 24:372–376
4. Matoba R, Niwa H, Masui S, Ohtsuka S, Carter MG, Sharov AA, Ko MS: Dissecting Oct3/4-regulated gene networks in embryonic stem cells by expression profiling. PLoS ONE 2006, 1:e26
5. Ivanova N, Dobrin R, Lu R, Kotenko I, Levorse J, DeCoste C, Schafer X, Lun Y, Lemischka IR: Dissecting self-renewal in stem cells with RNA interference. Nature 2006, 442:533–538
6. Takahashi K, Yamanaka S: Induction of pluripotent stem cells from mouse embryonic and adult fibroblast cultures by defined factors. Cell 2006, 126:1–14
7. Kim JB, Zaehres H, Wu G, Gentile L, Ko K, Sebastiano V, Araúzo-Bravo MJ, Ruau D, Han DW, Zenke M, Schöler HR: Pluripotent stem cells induced from adult neural stem cells by reprogramming with two factors. Nature 2008, 454:646–650
8. Jin T, Branch DR, Zhang X, Qi S, Youngson B, Goss PE: Examination of POU homeobox genes in breast cancer cells. Int J Cancer 1999, 81:104–112
9. Gidekel S, Pizov G, Bergman Y, Pikarsky E: Oct3/4 is a dose-dependent oncogenic fate determinant. Cancer Cell 2003, 4:361–370
10. Looijenga LH, Stoop H, de Leeuw HP, de Gouveia Brazao CA, Gillis AJ, van Roozendaal KE, van Zoelen EJ, Weber RF, Wolffenbuttel KP, van Dekken H, Honecker F, Bokemeyer C, Perlman EJ, Schneider DT, Kononen J, Sauter G, Oosterhuis JW: POU5F1 (OCT3/4) identifies cells with pluripotent potential in human germ cell tumors. Cancer Res 2003, 63:2244–2250
11. Atlasi Y, Mowla SJ, Ziaee SA, Bahrami AR: OCT-4, an embryonic stem cell marker, is highly expressed in bladder cancer. Int J Cancer 2007, 120:1598–1602
12. Yamaguchi S, Yamazaki Y, Ishikawa Y, Kawaguchi N, Mukai H, Nakamura T: EWSR1 is fused to POU5F1 in a bone tumor with translocation t(6;22)(p21;q12). Genes Chromosomes Cancer 2005, 43:217–222
13. Möller E, Stenman G, Mandahl N, Hamberg H, Mölne L, van den Oord JJ, Brosjö O, Mertens F, Panagopoulos I: POU5F1, encoding a key regulator of stem cell pluripotency, is fused to EWSR1 in hidradenoma of the skin and mucoepidermoid carcinoma of the salivary glands. J Pathol 2008, 215:78–86
14. Kawamura-Saito M, Yamazaki Y, Kaneko K, Kawaguchi N, Kanda H, Mukai H, Gotoh T, Motoi T, Fukayama M, Aburatani H, Takizawa T, Nakamura T: Fusion between CIC and DUX4 up-regulates PEA3 family genes in Ewing-like sarcomas with t(4;19)(q35;q13) translocation. Hum Mol Genet 2006, 15:2125–2137
15. Lundberg AS, Hahn WC, Gupta P, Weinberg RA: Genes involved in senescence and immortalization. Curr Opin Cell Biol 2000, 12:705–709
16. Narita M, Nũnez S, Heard E, Narita M, Lin AW, Hearn SA, Spector DL, Hannon GJ, Lowe SW: Rb-mediated heterochromatin formation and silencing of E2F target genes during cellular senescence. Cell 2003, 113:703–716
17. Ridley AJ, Hall A: The small GTP-binding protein rho regulates the assembly of Focal adhesions and actin stress fibers in response to growth factors. Cell 1992, 70:401–410
18. Hanahan D, Weinberg RA: The hallmarks of cancer. Cell 2000, 100:57–70
19. Seiki M: The cell surface: the stage for matrix metalloproteinase regulation of migration. Curr Opin Cell Biol 2002, 14:624–635
20. Seiki M, Mori H, Kajita M, Uekita T, Itoh Y: Membrane-type 1 matrix metalloproteinase and cell migration. Biochem Soc Symp 2003, 70:253–262
21. Seiki M, Koshikawa N, Yana I: Role of pericellular proteolysis by membrane-type 1 matrix metalloproteinase in cancer invasion and angiogenesis. Cancer Metastasis Rev 2003, 22:129–143
22. Bonuccelli G, Casimiro MC, Sotgia F, Wang C, Liu M, Katiyar S, Zhou J, Dew E, Capozza F, Daumer KM, Minetti C, Milliman JN, Alpy F, Rio MC,

Tomasetto C, Mercier I, Flomenberg N, Frank PG, Pestell RG, Lisanti MP: Caveolin-1 (P132L), a common breast cancer mutation, confers mammary cell invasiveness and defines a novel stem cell/metastasis-associated gene signature. Am J Pathol 2009, 174:1650–1662
23. Boire A, Covic L, Agarwal A, Jacques S, Sherifi S, Kuliopulos A: PAR1 is a matrix metalloprotease-1 receptor that promotes invasion and tumorigenesis of breast cancer cells. Cell 2005, 120:303–313
24. Gumienny TL, Brugnera E, Tosello-Trampont AC, Kinchen JM, Haney LB, Nishiwaki K, Walk SF, Nemergut ME, Macara IG, Francis R, Schedl T, Qin Y, Van Aelst L, Hengartner MO, Ravichandran KS: CED-12/ELMO, a novel member of the CrkII/Dock180/Rac pathway, is required for phagocytosis and cell migration. Cell 2001, 107:27–41
25. Wilson EM, Oh Y, Hwa V, Rosenfeld RG: Interaction of IGF-binding protein-related protein 1 with a novel protein, neuroendocrine differentiation factor, results in neuroendocrine differentiation of prostate cancer cells. J Clin Endocr Metab 2001, 86:4504–4511
26. Chien J, Staub J, Hu SI, Erickson-Johnson MR, Couch FJ, Smith DI, Crowl RM, Kaufmann SH, Shridhar V: A candidate tumor suppressor HtrA1 is downregulated in ovarian cancer. Oncogene 2004, 23:1636–1644
27. Markowitz S, Wang J, Myeroff L, Parsons R, Sun L, Lutterbaugh J, Fan RS, Zbrowska E, Kinzler KW, Vogelstein B, Brattain M, Willson JKV: Inactivation of the type II TGF-beta receptor in colon cancer cell with microsatellite instability. Science 1995, 268:1336–1338
28. He B, You L, Uematsu K, Zang K, Xu Z, Lee AY, Costello JF, McCormick F, Jablons DM: SOCS-3 is frequently silenced by hypermethylation and suppresses cell growth in human lung cancer. Proc Natl Acad Sci USA 2003, 100:14133–14138
29. Lagos-Quintana M, Rauhut R, Yalcin A, Meyer J, Lendeckel W, Tuschl T: Identification of tissue-specific microRNAs from mouse. Curr Biol 2002, 12:735–739
30. Aravin AA, Lagos-Quintana M, Yalcin A, Zavolan M, Marks D, Snyder B, Gaasterland T, Meyer J, Tuschl T: The small RNA profile during Drosophila melanogaster development. Dev Cell 2003, 5:337–350
31. Suh MR, Lee Y, Kim JY, Kim SK, Moon SH, Lee JY, Cha KY, Chung HM, Yoon HS, Moon SY, Kim VN, Kim KS: Human embryonic stem cells express a unique set of microRNAs. Dev Biol 2004, 270:488–498
32. Barroso-del Jesus A, Romero-López C, Lucena-Aguilar G, Melen GJ, Sanchez L, Ligero G, Berzal-Herranz A, Menendez P: Embryonic stem cell-specific miR302-367 cluster: human gene structure and functional characterization of its core promoter. Mol Cell Biol 2008, 28:6609–6619
33. Sherr CD, Roberts JM: CDK inhibitors: positive and negative regulators of G1-phase progression. Genes Dev 2001, 13:1501–1512
34. Yamaguchi H, Condeelis J: Regulation of the actin cytoskeleton in cancer cell migration and invasion. Biochim Biophys Acta 2007, 1773:642–652
35. Carreira S, Goodall J, Denat L, Rodriguez M, Nuciforo P, Hoek KS, Testori A, Larue L, Goding CR: Mitf regulation of Dia1 controls melanoma proliferation and invasiveness. Genes Dev 2006, 20:3426–3439
36. Fromique O, Hamidouche Z, Marie PJ: Nlockade of the RhoA-JNK-c-Jun-MMP2 cascade by atorvastatin reduces osteosarcoma cell invasion. J Biol Chem 2008, 283:30549–30556
37. Sugimoto K, Ishibashi T, Sawamura T, Inoue N, Kamioka M, Uekita H, Ohkawara H, Sakamoto T, Sakamoto N, Okamoto Y, Takuwa Y, Kakino A, Fujita Y, Tanaka T, Teramoto T, Maruyama Y, Takeishi Y: LOX-1-MT1-MMP axis is crucial for RhoA and Rac1 activation induced by oxidized low-density lipoprotein in endothelial cells. Cardiovasc Res 2009, 84:127–136
38. Besson A, Gurian-West M, Schmidt A, Hall A, Roberts JM: p27Kip1 modulates cell migration through the regulation of RhoA activation. Genes Dev 2004, 18:862–876
39. Weinberg RA: Multistep tumorigenesis: the biology of cancer. Edited by RA Weinberg. Garland Science, New York, NY 2007, pp 399–462
40. Lee J, Kim JY, Kang IY, Kim HK, Han YM, Kim J: The EWS-Oct-4 fusion gene encodes a transforming gene. Biochem J 2007, 406:519–526
41. Boyer LA, Lee TI, Cole MF, Johnstone SE, Levine SS, Zucker JP, Guenther MG, Kumar RM, Murray HL, Jenner RG, Gifford DK, Melton DA, Jaenisch R, Young RA: Core transcriptional regulatory circuitry in human embryonic stem cells. Cell 2005, 122:947–956
42. Loh YH, Wu Q, Chew JL, Vega VB, Zhang W, Chen X, Bourque G, George J, Leong B, Liu J, Wong KY, Sung KW, Lee CW, Zhao XD, Chiu KP, Lipovich L, Kuznetsov VA, Robson P, Stanton LW, Wei CL, Ruan Y, Lim B, Ng HH: The Oct4 and Nanog transcription network regulates pluripotency in mouse embryonic stem cells. Nat Genet 2006, 38:431–440
43. Greer Card DA, Hebbar PB, Li L, Trotter KW, Komatsu Y, Mishina Y, Archer TK: Oct4/Sox2-regulated miR-302 targets cyclin D1 in human embryonic stem cells. Mol Cell Biol 2008, 28:6426–6438